UNIVERSITÀ DEGLI STUDI DI PADOVA

DIPARTIMENTO DI BIOLOGIA

Corso di Laurea magistrale in Molecular Biology

TESI DI LAUREA

Cardiac defects and Wnt/β-catenin signalling impairment in Lgals3a zebrafish mutants

Relatore: Prof.ssa Natascia Tiso
Dipartimento di Biologia

Correlatore: Dott. Giovanni Risato
Dipartimento di Scienze Cardio-Toraco-Vascolari e Sanità Pubblica

Laureanda: Almıla İzbırak

ANNO ACCADEMICO 2021/2022

TABLE OF CONTENTS

ABSTRACT 1

1. INTRODUCTION 2

1.1 Arrhythmogenic Cardiomyopathy 2

1.1.1 Genetic background 3

1.1.2 Pathology of AC 5

1.1.3 Desmosomes 7

1.2 Molecular Pathogenesis of AC 8

1.2.1 The Wnt/β-catenin signalling Pathway 9

1.2.1.1 Wnt signalling in the heart. 11

1.2.2 Hippo/YAP-TAZ signalling 11

1.2.3 Loss of cardiomyocytes 12

1.2.4 Inflammation and Fibrosis 13

1.3 Galectins 14

1.3.1 Galectin-3 15

1.3.2 Galectin-3 gene and protein structure 16

1.3.3 The biological functions of Gal-3 18

1.3.3.1 Apoptosis. 18

1.3.3.2 Cell Adhesion. 19

1.3.3.3 Wnt/β-catenin signalling. 20

1.4 Zebrafish as a model organism 21

1.4.1 Zebrafish for the study of AC 23

1.4.2 Galectin-3 in Zebrafish 24

2. MATERIALS AND METHODS 26

2.1 Maintenance of zebrafish lines 26

2.2 *Lgals3a* line 27

2.3 Genotyping of *lgals3a* line 27

2.4 Western Blotting 28

2.5 Morphological analysis 29

2.6 Heart rate estimate at larval stage 29

2.7 RNA isolation and real-time PCR (qRT-PCR) 30

2.8 Immunofluorescence analysis 31

2.9 Acridine Orange staining 32
2.10 Mortality rate assay 32
2.11 Statistical analysis 32
3. RESULTS 33
3.1 Genotyping 33
3.2 *Lgals3a* mRNA expression 34
3.3 Desmoplakin protein expression 35
3.4 Wnt/β-catenin signalling suppression 36
3.5 Wnt target genes expressions 37
3.6 YAP-TAZ target genes expressions 37
3.7 Morphological analysis 38
3.8 Heart rate estimation 41
3.9 Heart chambers dilation 41
3.10 Immunofluorescence analysis 43
3.11 Acridine Orange staining 44
3.12 Survival rate analysis 45
4. DISCUSSION 47
5. CONCLUSIONS AND FUTURE PERSPECTIVES 52
REFERENCES 54

ABSTRACT

Arrhythmogenic cardiomyopathy (AC) is an inherited disease, mostly caused by mutations in genes that encode desmosomal proteins. However, recent evidence suggests a potential causative role played by reduced Galectin-3 expression in early AC onset. Thereby, we aimed to characterise a zebrafish line with a frameshift mutation in the gene encoding for Galectin-3 (*lgals3a*). Using a specific transgenic zebrafish line and qPCR analysis, we demonstrated that canonical Wnt/β-catenin signalling, a pathway frequently dysregulated in AC, is significantly suppressed in *lgals3a* -/- mutant larvae, similar to what observed in other AC models. The expression of Desmoplakin protein was also found to be reduced by Western blot analysis. Moreover, these larvae exhibited developmental defects and morphological alterations in their cardiac region with a 35% penetrance, among which we revealed cardiac chamber dilation, pericardial effusion and bradycardia phenotype. The dilation of the heart was maintained in 1-year-old mutant zebrafish. Lgals3a mutation also induced cell death and inflammatory response in the larval cardiac region. In parallel, these animals showed ~17% decrease in their life expectancy compared to their WT counterparts. In summary, the Lgals3a-KO zebrafish line recapitulates many AC features observed in human patients, pointing at zebrafish as a suitable model to study Galectin-3 as a remarkable modulator of Wnt/β-catenin signalling and AC-like phenotypes.

1. INTRODUCTION

1.1 Arrhythmogenic Cardiomyopathy

Arrhythmogenic cardiomyopathy (AC) is a rare autosomal dominant disease characterised by progressive myocardial fibro-fatty replacement, which leads to ventricular arrhythmias, predisposing patients to sudden cardiac death (SCD). Although rare, a significant proportion of deaths occurring in the young adults and athletes are AC-related. Moreover, athletes who are genetically predisposed have a 5-fold higher risk of developing AC and SCD compared to non-athletes (Hoorntje et al., 2017). The molecular pathogenesis giving rise to AC concerns, to a great degree, the variants of genes encoding for desmosomal proteins in the myocardium (50% of AC cases), where genetic predisposition remains the main underlying cause of AC (~50% of the cases have family history).

Currently, it is evident that this disease falls on a spectrum extending from the original definition, arrhythmogenic right ventricular cardiomyopathy (ARVC), to more recently identified forms such as left-dominant or biventricular ones (Hoorntje et al., 2017). This led to the broad term of AC, which incorporates all the phenotypic expressions of the disease. Prevalence of AC is estimated to be between 1:2,000 and 1:5,000 in some European countries (e.g. Italy, Germany and Netherlands) and in the general population respectively (Corrado et al., 2017). Moreover, there seems to be a difference in the clinical presentation (i.e. observed in baseline ECG (electrocardiogram), ventricular arrhythmias, etc.) of AC between males and females, with males having a more severe form of the disease at higher incidence, despite a similar prevalence of carrier status among the sexes (Pilichou et al., 2016). Such presentations include palpitations, syncopal episodes, ventricular arrhythmias and cardiac arrest, becoming clinically overt in the second-fourth decade of life in majority of the cases. This has been attributed to the effect of sex hormones on the phenotypic expression of the disease or to the differences in the duration and intensity of exercise due to gender-related differences (Pilichou et al., 2016).

AC-related deaths are mainly due to the challenges presented by early diagnosis. Both clinically and genetically, AC is a heterogeneous disease whose symptoms can range from almost (if not entirely) asymptomatic (i.e. concealed initial phase) to severe. Its primary pathological features, the presence of myocardial adipocytes and the thinning of the ventricular myocardium, are frequently the only diagnostic

factors, growing the frequency of misdiagnosis, which can lead to false treatment and even death (Migliore et al., 2021).

Preventing SCD, containing heart failure (HF) events, attenuating arrhythmias and deceleration of disease progression are the main objectives in AC management. To choose the most suitable therapy, symptoms and risk profiles of the individual patients must be properly evaluated. Even though implantable cardioverter defibrillators (ICDs) possess significant risks (e.g. death) due to complications regarding the device itself and improper shocks, ICD therapy is the only promising life-sustaining treatment up-to-date (Pilichou et al., 2016). An alternative to ICD is subcutaneous ICD; this is a popular choice among patients with limitations in vascular access and high risk of infection. Conventional pharmacologic therapy includes the use of beta-blockers to impede ventricular arrhythmias arising from physical effort and to lower ventricular wall stress, slowing down the progression of disease (Migliore et al., 2021). The use of anti-arrhythmic and anti-HF drugs has also been reported. Among novel pharmacological options, SB216763, has been reported to ameliorate the pathological condition in animal AC models by inhibiting glycogen synthase kinase 3β enzyme (GSK-3β) and consequently upregulating the Wnt/β-catenin pathway expression (Migliore et al., 2021). Undoubtedly, prolonged use of SB216763 introduces the risk of cancer development, putting such drugs in jeopardy.

1.1.1 Genetic background

In the majority of the AC cases (~50%), the progressive replacement of the ventricular myocardium with fibro-fatty tissue is caused by mutations in genes encoding for cardiac desmosomal proteins in the intercalated discs (IDs) of the heart (Calore et al., 2014) (Table 1.1). However, non-desmosomal pathogenic variants have also been discovered in a few patients and model animals, owing to numerous genetic approaches, pointing towards genetic heterogeneity in AC.

Desmosomal mutations are mostly inherited in an autosomal dominant manner with an age-related and incomplete penetrance, also showing variable expressivity (Calore et al., 2014). Among these, the most prevalent are heterozygous plakophilin-2 (PKP2) mutations (followed by desmoplakin ones) that lead to premature termination of the functional protein product and/or aberrant splicing. Non-desmosomal mutations have also been found in a small number of individuals (1-3%) (Table 1.1). The earliest of them was the p.S358L founder mutation discovered in individuals from Canada and Europe in transmembrane protein 43 (TMEM43) gene (Rampazzo et al., 2014). Furthermore, desmin, titin, lamin A/C, phospholamban, $Na_V1.5$, and filamin C are only a few of the many genes linked to

different forms of cardiomyopathies and arrhythmia syndromes that have been shown to contain pathogenic mutations.

Table 1. List of genetic mutations implicated in AC (modified from Corrado et al., 2017).

Gene	Encoded Protein	Subcellular Localisation
JUP	Plakoglobin	Desmosome
DSP	Desmoplakin	Desmosome
PKP2	Plakophilin-2	Desmosome
DSG2	Desmoglein-2	Desmosome
DSC2	Desmocollin-2	Desmosome
TMEM43	Transmembrane protein 43	Nuclear envelope
LMNA	Lamin A/C	Nuclear envelope
DES	Desmin	Intermediate filament
CTNNA3	Alpha-T-catenin	Area composita
PLN	Phospholamban	SERCA
TGFB3	Transforming growth factor-3	Growth factor
TTN	Titin	Sarcomere
SCN5A	Sodium voltage-gated channel ($Na_V1.5$)	Sodium channel
CDH2	Cadherin C	Area composita

Even though most AC cases have been proven to carry disease-causing variants, it has come to light that a considerable number of genetic determinants are yet to be identified, since 35-50% of patients who suffer from AC have no identified variants (Hoorntje et al., 2017). This is no surprise considering the heterogeneous nature of AC which indicates both polygenic and environmental factors exerting an influence on the phenotypic expression of the disease. Nevertheless, the phenotypic variability can be, in part, explained by the presence of compound/digenic heterozygosity, which was demonstrated to be ~25% in AC-causing desmosomal gene mutation carriers. Although rare, there are also homozygous mutations. These findings give credence to the idea that other genetic and/or environmental variables may have modifying effects (Hoorntje et al., 2017). In addition, it has been revealed that the onset of disease, progression and prognosis in AC are determined by comorbidities, age and epigenetic factors. Moreover, dilated cardiomyopathy and

Brugada syndrome clinically overlap with AC (Corrado et al., 2017), suggesting pleiotropy or involvement of the same genetic variants. Therefore, it is of importance to identify unknown or overlooked mediators of AC with the aim of extending our current understanding of the molecular genetics and pathogenesis of this disease.

Recently, in an effort to uncover molecular pathways underlying early AC, Cason et al. identified 29 differentially expressed genes where Lgals3/Galectin-3 (Gal-3) was shown to have reduced cardiac expression in transgenic mice overexpressing Desmoglein2-N271S mutation and 3 AC patients who suffered SCD at early disease stages (Cason et al., 2021). Further research identified 4 rare missense variants of *LGALS3* in AC patients negative for disease-related gene variants and one of them was found to be located at the conserved carbohydrate recognition domain (CRD), which conferred the loss of its function. Moreover, they discovered that *LGALS3* rare variants were present in 4% of the cases in a large AC cohort.

The following sections move on to describe in greater detail the relevance of the CRD region and the implications of Gal-3 in AC disease context.

1.1.2 Pathology of AC

Although extensive substitution of the myocardium with fatty-fibrous tissue is considered the hallmark attribute of AC, this feature is more apparent at the advanced disease stage. Cardiomyocyte loss due to desmosomal instability affects the structural integrity of the heart, but it also alters the intercellular signal transduction, leading to electrophysiological abnormalities. Patients with AC often exhibit palpitations, pre-syncope, syncope, or SCD between the ages of 13 and 40.

AC progression is divided into four stages: (i) an early, concealed stage in which patients are free of symptoms with no or subtle right ventricle (RV) structural changes, with a risk of SCD. An overt stage (ii) with ventricular arrhythmia (VA) symptoms (palpitations, syncope, etc.) and evident RV structural remodelling followed by a progressive stage (iii) that results in RV fibro-fatty replacement of the myocardium, presence of congestive HF (still under control) with fluid accumulation, ascites, oedema, and dyspnoea. The final biventricular stage (iv) is characterised by LV involvement and global dilation, together with HF (Corrado et al., 2017).

SCD may develop at any point during the course of the disease because of electrical problems concerning impulse generation and propagation. This is noteworthy since it also covers the preclinical stage, upon which arrhythmias and/or SCD, which are

typically the first signs of the condition, are prominent. Determining the clinical characteristics that indicate an early arrhythmic risk has thus been the focus of numerous studies. Depolarization delay, cardiac syncope, premature ventricular complex frequency, deformation imaging, and biomarkers are some examples of possible arrhythmic indicators that have been studied (Pilichou et al., 2016).

Wall thinning and aneurysmal dilatation, which are located mainly in the inflow tract (sub-tricuspid region), outflow tract (infundibular region), and apex ("triangle of dysplasia"), are exacerbated by the progression of fibro-fatty scar tissue from the epicardium toward the endocardium, with involvement of the RV wall in particular (Corrado et al., 2017) (Figure 1.1). These pathological features undoubtedly worsens cardiac arrhythmias. End-stage disease that results in HF typically manifests as massive bi-ventricular chamber dilatation and many free-wall aneurysms. Indeed, genotype-phenotype correlation studies have shown that AC might have a vastly greater phenotypic spectrum than initially believed (Corrado et al., 2017). The pathologic characteristics extend from hearts with severe biventricular disease involvement to anatomically normal hearts, where only a thorough histopathologic examination can detect AC symptoms in one or both ventricles.

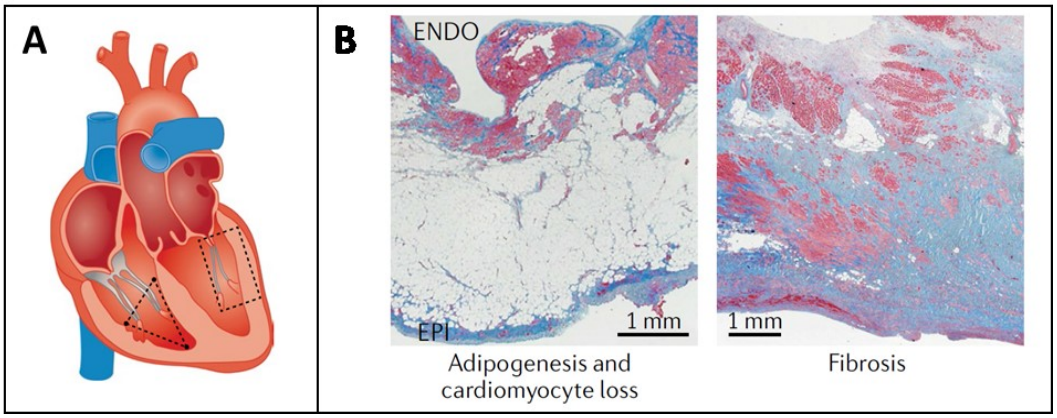

Figure 1.1. Histopathological features of AC. A) Illustration depicting the commonly affected ventricular regions in AC. B) Histological features of AC; adipogenesis, cardiomyocyte replacement and fibrosis. ENDO, endocardium; EPI, epicardium (modified from Austin et al., 2019).

Moreover, patchy inflammatory infiltrates -primarily T lymphocytes- are frequently encountered alongside dying myocytes, pointing to an immunological basis for the pathophysiology. Indeed, the majority of hearts examined at autopsies were found to have myocardial inflammation, where cardiomyocyte necrosis was demonstrated to be the primary cause of myocardial damage in an AC transgenic animal model, resulting in progressive myocardial loss and inflammatory response (Hoorntje et

al., 2017) (Corrado et al., 2017). The proper interpretation of the autopsy results is crucial since the proband's post-mortem diagnosis of AC allows for cascade screening of surviving relatives and risk-based preventive therapy for SCD (Corrado et al., 2017). An inaccurate AC diagnosis might expose family members to the danger of over-diagnosis, inappropriate defibrillator installation, as well as expensive and time-consuming clinical assessment.

1.1.3 Desmosomes

Desmosomes, adherens junctions, and gap junctions all exist in mixed-type complex known as the area composita that is situated at the intercalated discs (IDs) (Figure 1.2). This area is where cardiomyocytes are structurally and electrically connected to each other. Cardiomyocytes are strictly interconnected at their ends via their IDs, a complex region containing multiple kinds of intercellular junctions required for electrical and mechanical interactions between adjacent cells, thus, for proper heart function (Calore et al., 2014). Although cardiomyocyte ID has historically been represented as a collection of distinct units, recent research suggests that it should be viewed as a single functional unit in which macromolecular complexes interact mechanically and electrically to preserve cardiomyocyte adhesion and synchrony (Rampazzo et al., 2014).

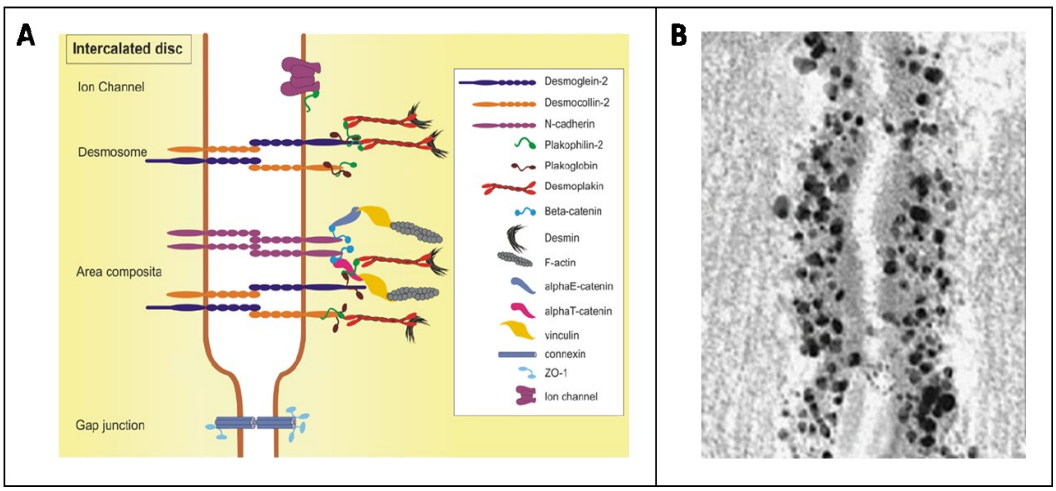

Figure 1.2. Molecular composition and organisation of the ID, connecting the cardiomyocytes. A) Illustration of the ID molecular composition; proteins are depicted in the box on the right. B) Immuno-electron micrographs of a cross-section of the myocardium of the human heart, showing DSP in the ID (modified from Rampazzo et al., 2014 and Calore et al., 2014).

Cardiac desmosomes are complex proteins that provide mechanical connections between cardiomyocytes in IDs, maintaining the structural integrity. In particular, they mediate mechanical tethering of neighbouring cells by linking their intermediated filaments (IFs) to form a cytoskeletal network, especially in tissues exposed to mechanical forces, such as the heart and skin. The cardiac desmosome consists of desmoglein-2 (DSG2) and desmocollin-2 (DSC2), attached to armadillo proteins called plakoglobin (JUP) and plakophilin-2 (PKP2) and cytolinker protein desmoplakin (DSP) which interacts with desmin IFs in cardiomyocytes (Garrod & Chidgey, 2008).

DSG2 and DSC2, the two transmembrane proteins from the cadherin family, facilitate intercellular adhesion and act as a scaffold for the establishment of the desmosomal wall through their cytoplasmic domains. These cytoplasmic domains do in fact serve as a binding site for the armadillo family members JUP and PKP2, which then interact with DSP isoforms, in which through their C termini, complete the link with desmin IFs. For myocardial integrity, this interaction of IFs with desmosomes is crucial since it distributes the tensile strength provided by the IF cytoskeleton throughout the entire issue. Desmosomal plaque and IF scaffolding are connected by DSP in the desmosome-intermediate filaments complexes (DIFCs). Desmosomal cadherins cross the membrane with their C-terminal domains located in the plaque and with their N-terminal domains, link the two parts of the desmosome together in the intercellular space (Garrod & Chidgey, 2008).

Tissues that are subjected to mechanical stress may disintegrate in response to the collapse of the desmosomal adhesion. DIFC preserves the integrity of such tissues. DIFC is composed by three parts: two intracellular and one intercellular. Although the two intracellular regions of the DIFC have been extensively studied, limited information is available on adhesive binding mechanisms. As demonstrated by some human disorders of the epidermis, each one of these three parts of the DIFC has to be equally able to withstand mechanical disruption; failure in one single component is incredibly damaging (Garrod & Chidgey, 2008).

1.2 Molecular Pathogenesis of AC

Although the pathophysiology of this rare type of cardiomyopathy is still not completely understood, some predisposing factors are now well known. Attention has been mostly focused on desmosomes, the intercellular junctions expressed by cardiomyocytes, accounting for most of the AC-related mutations. Loss of adhesion among cardiac myocytes, which drives their detachment and apoptosis and the subsequent replacement by fibro-fatty tissue, is the most straightforward theory for

how desmosomal mutations lead to AC. It is commonly accepted that exercise worsens cell adhesion, with the thinner-walled RV suffering more damage than the LV (Hoorntje et al., 2017). Clinical pathology research has revealed that AC is the key contributor in sport-related SCD. A number of animal models have emphasised the contribution of exercise to the pathogenesis of AC by exacerbating the phenotypic condition (Hoorntje et al., 2017).

The loss of right ventricular myocardium and the replacement with fibrous and fatty tissue is the characteristic histologic hallmark of AC, as previously mentioned. Cardiomyocyte loss, fibrosis, adipogenesis, inflammation and arrhythmogenesis are the main manifestations of AC that are associated with pathogenic mutations. Several signalling pathways, including Wnt, Hippo-YAP/TAZ and transforming growth factor beta (TGFβ) have been linked to these AC phenotypes.

1.2.1 The Wnt/β-catenin signalling Pathway

The Wnt/β-catenin signalling is a key signal transduction pathway that plays a major part in the development of a wide range of species. This pathway has been preserved throughout evolution, controlling cell proliferation, morphology, motility, axis formation and so on. In the absence of Wnt ligands, the primary downstream signalling molecule, β-catenin, together with APC and Axin, is phosphorylated by GSK-3β and CKI (collectively called β-catenin destruction complex). This phosphorylation drives β-catenin towards ubiquitination and proteasomal degradation. In response to Wnt ligands, upon activation and disruption of the destruction complex, β-catenin translocates into the nucleus. There, it binds and coactivates the TCF/LEF1 transcription factors which bind to DNA and mediate transcription of Wnt target genes including c-myc and cyclin D1, and subsequent cell proliferation and growth (Lorenzon et al., 2017). This is supported by numerous studies, which demonstrate that the dysregulation of the pathway leads to tumour development in a variety of tissues.

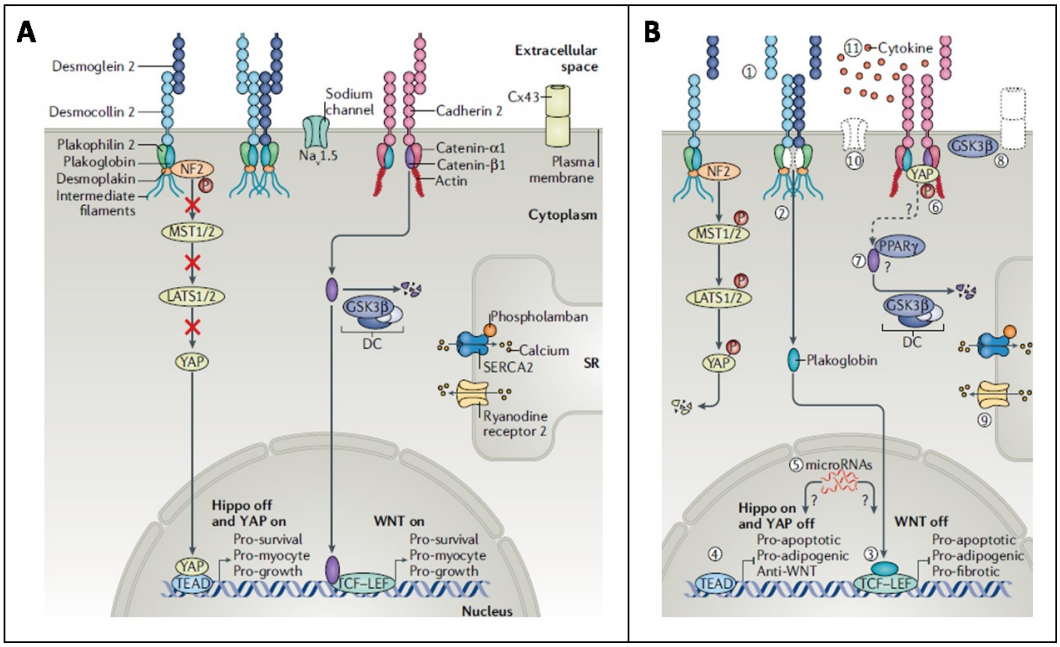

Figure 1.3. Molecular mechanisms of AC. A) Healthy cardiomyocytes with stable ID arrangement; appropriate regulation of the key signalling pathways including Wnt/β-catenin and Hippo pathways. B) Disruption of desmosomal integrity and weakened intercellular junctions in response to desmosomal mutations; dysregulation of the signalling pathways due to loss of cell adhesion and plakoglobin (JUP) release (modified from Austin et al., 2019).

In response to the desmosomal instability arising from AC-related mutations, JUP (also called γ-catenin) is released from the cell surface to the nucleus. JUP competes with β-catenin for nuclear translocation and canonical Wnt/β-catenin signalling activation (Austin et al., 2019) (Lorenzon et al., 2017) (Figure 1.3). This was demonstrated by using short interfering RNA to reduce the level of DSP in a myocyte cell culture system to show for the first time how desmosome disruption downregulates canonical Wnt signalling and the activity of Wnt transcription factors (Corrado et al., 2017). Additionally, heterozygous DSP-deficient rodents were found to mimic human AC with relatively high nuclear JUP and the presence of fibrosis and adipogenesis in the ventricular myocardium, as well as attenuated Wnt signalling (Corrado et al., 2017).

The current AC treatment research is mainly focused on the development of new drugs that could potentially impede the underlying molecular processes of AC. Thereby, most therapies are aimed at upregulating the Wnt signalling. SB216763, an inhibitor of GSK-3β, has been found by Asimaki et al. to ameliorate the pathophysiological features of AC in zebrafish and mice by promoting Wnt signalling. Following therapy, improvements in cardiac histology, arrhythmia, function, and survival were observed (Asimaki et al., 2014). Inhibition of GSK-3β

promotes the Wnt pathway since GSK-3β is a major negative regulator (repressor) of canonical Wnt signalling. Furthermore, desmosome mutations are associated with reduced cytoplasmic localization of GSK-3β and its redistribution in the IDs, (Chelko et al., 2016) - in contrast to other types of cardiomyopathy - which indicates a more prominent function for GSK-3β and clearly demonstrates that this enzyme has a greater role in the pathophysiology of AC.

1.2.1.1 Wnt signalling in the heart.

In both invertebrates and vertebrates, Wnt/β-catenin signalling is important for the majority of embryonic developmental processes, providing one of the key embryonic signals that controls body axis determination, embryonic morphology, cell proliferation, nervous system and lymphatic system in vertebrates.

As regards the heart, there seems to be an overall effect of numerous players such as the Wnt growth factors, Notch and Hippo proteins on the processes required to develop a healthy heart. Specifically, the Wnt pathway was shown to be crucial for myocardial specification and proliferation, cardiac morphogenesis, cardiac valve formation, as well as endothelial and vascular smooth muscle cell proliferation. In this regard, early suppression of Wnt signalling leads to deformities in the outflow tract and chambers, along with malformations in other morphological regions. Furthermore, non-canonical Wnt signalling was reported to drive the differentiation of cardiac precursors whereas canonical Wnt signalling regulates the proliferative potential of the differentiated cardiomyocytes and keeps the cardiac precursors in a proliferative and precursor state. Therefore, a proper equilibrium between these pathways is crucial for epicardium differentiation and epicardial cell growth (Lorenzon et al., 2017). Wnt/β-catenin signalling dysregulation in the adult has been mostly associated with numerous human diseases such as cancer.

1.2.2 Hippo/YAP-TAZ signalling

AC pathophysiology, in many cases, has been linked to adipogenesis fuelled by the Hippo/YAP-TAZ signalling pathway. The name “hippo” arises from the findings that loss of function mutations in the core elements of the pathway can result in hippopotamus-like overgrowth. The Hippo pathway is a key regulator of organ size, cell proliferation, survival and differentiation, typically stimulated because of mechanical signals or cell-cell contacts. Briefly, YAP and TAZ are transcriptional co-activators that enhance gene expression responsible for driving cell proliferation and resistance to apoptosis. These downstream effectors of Hippo signalling are

phosphorylated and inhibited by a kinase cascade (MTS1/2 and LATS1/2) upon Hippo pathway activation (Chen et al., 2014). Following phosphorylation, YAP and TAZ are sequestered in the cytoplasm, leaving them incapable of exerting their transcriptional activities in the nucleus. Another consequence of YAP-TAZ accumulation in the cytoplasm is the suppression of the canonical Wnt pathway since YAP-TAZ are involved in the β-catenin destruction complex (Chen et al., 2014).

In the context of AC, Merlin (NF2), which acts upstream of the Hippo kinases, is another component of the IDs. It was demonstrated by Chen et al. that the mutations involving proteins that localise to the IDs disrupt the structural integrity of the area composita, but also alter the signalling pathways that are controlled at the level of the IDs. Thus, it was confirmed that desmosome mutations (i.e. PKP2) affect the Hippo pathway and hence lead to the onset of fibro-adipose tissue in the heart, following the dysregulation of NF2 by the compromised distribution of phosphorylated protein kinase C to the genetically perturbed IDs (Figure 1.3) (Lorenzon et al., 2017) (Chen et al., 2014).

1.2.3 Loss of cardiomyocytes

The loss of cardiomyocytes which leads to cardiac muscle atrophy and myocardial thinning in AC is in part linked to cell death mechanisms such as apoptosis (programmed cell death), necrosis and necroptosis (programmed necrosis). These mechanisms arise from weakened intercellular junctions and inflammation. Indeed, histological analysis of AC hearts usually demonstrates the cardiomyocyte loss coupled with patchy inflammation (Figure 1.4) (Austin et al., 2019).

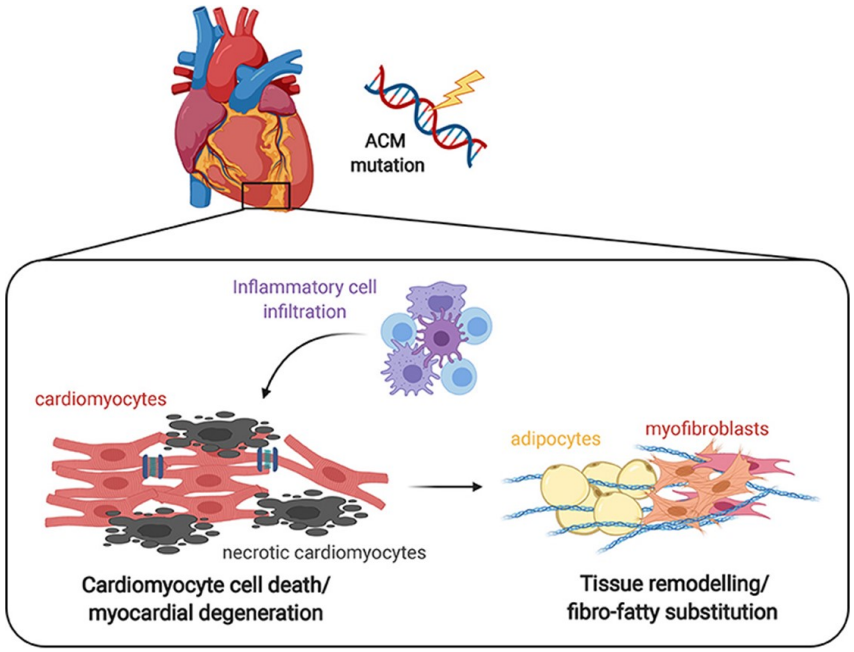

Figure 1.4. The interplay of inflammation and myocardial cell death in AC. Myocardium is substituted by fibro-fatty tissue in response to cardiac cell death (apoptosis and necrosis) and inflammatory cell accumulation (Meraviglia et al., 2021).

In detail, apoptotic cell death was shown to take part in AC, as evidenced by several studies involving desmosomal mutations, where TUNEL analysis was used to stain for apoptosis. Furthermore, canonical Wnt pathway dysregulation, arising from the JUP release due to desmosomal instability and subsequent signalling suppression contributes to apoptotic cardiomyocyte loss in AC. In addition, the mechanical stretch of myocytes during intensive exercise may promote damage in the cells and exacerbate apoptosis due to desmosome fragility (Austin et al., 2019).

However, the contribution of necrosis and necroptosis is less understood. In fact, cardiomyocyte death is often paired with inflammation, a process that is not necessarily linked to apoptosis, even though many AC samples are stained by TUNEL assay. This suggests a necrosis-related mechanism of cell death. Indeed, researchers have demonstrated necrosis features in two mice models of AC (Austin et al., 2019).

1.2.4 Inflammation and Fibrosis

Regeneration and fibrosis are both significantly promoted by tissue damage and inflammation. In response to damage, the cells of the innate and adaptive immune systems are recruited to the site of the damage and the build-up of extracellular

matrix (ECM) elements triggers fibrosis. Myocardial fibrosis is involved in several cardiac diseases and AC is no exception. Chronic cardiomyocyte loss, the recruitment of inflammatory cells and the activation of fibroblasts all contribute to scarring in the heart in AC (Figure 1.4) (Austin et al., 2019).

AC patients have elevated levels of circulating cytokines in their blood, as well as other inflammatory cell infiltrates such as macrophages. This phenomenon is thought to be induced by the progressive loss of the myocardium due to desmosomal mutations where experiments involving such mutants demonstrate that structural damage and cell death stimulate the recruitment of inflammatory cells such as IL-6 and tumour necrosis factor alpha (TNFα) which contribute to disease progression (Austin et al., 2019).

Mechanisms controlling the fibro-fatty replacement of the myocardial tissue in AC is still of debate. However, TGFβ signalling pathway is known to be a central mediator of fibrogenesis and especially its upregulation, is associated with numerous human diseases involving fibrotic remodelling. The interplay of both canonical and non-canonical TGFβ signalling seems to induce the events leading to fibrosis in AC. The canonical pathway on one hand, was demonstrated to promote the expression of ECM proteins and suppress matrix metalloproteinases whereas the non-canonical pathway exerts its role through mitogen-activated protein kinase (MAPK) dependent mechanisms. Furthermore, mutations involving the key players of the canonical signalling (e.g. TGFβ1 and TGFβ3) have been linked with AC fibrotic phenotype via both non-canonical dependent and independent mechanisms (Austin et al., 2019).

1.3 Galectins

Galectins are a family of β-galactoside carbohydrate binding proteins encoded by the *LGALS* gene family in humans and are involved in a wide range of physiological processes, including signalling, cell migration and adhesion, inflammation, apoptosis and mRNA stability (Sciacchitano et al., 2018). Several significant pathologies such as organ fibrosis, diabetes, cancer and cardiac disease are linked to galectins on a frequent basis. Being expressed in multiple tissues and compartments, with potential complementation of each other by the different members of the family, these aspects make galectins a challenging area of research.

Initially, galectins were found while looking for proteins that could decode complex cell-surface glycans based on their galactoside binding ability (Johannes et al., 2018). They are classified as a family based on conserved galactoside-binding sites

that are present in their distinctive 130 amino acid (aa) carbohydrate recognition domains (CRDs), the structural hallmark of galectins (Johannes et al., 2018). It was eventually revealed that galectins function both intra and extracellularly, as well as in the nucleus (Sciacchitano et al., 2018). Synthesised in the cytoplasm, galectins reach their galactoside ligands following a non-classical secretion that bypasses the Golgi complex (Sciacchitano et al., 2018). Galectins do indeed interact with a variety of non-galactose-containing binding partners, and their CRDs (or other components) contain non-carbohydrate binding sites. The expression pattern of galectins differs between different cell types and tissues even though all cells often express a cytosolic concentration of galectins to some extent (Johannes et al., 2018).

Structurally, galectins are small soluble proteins that contain one or two CRDs. The 15 putative members of the family are divided into three types based on domain organisation; the 'prototype' galectin-1, -2, -5, -7, -10, -11, -13, -14 and -15 which have one CRD; the chimeric galectin-3, containing a single C-terminal CRD and an amino-terminal polypeptide tail region; the tandem repeat galectins galectin-4, -6, -8, -9, and -12, which have two CRDs, make up the core group of vertebrate galectins (Sciacchitano et al., 2018).

Galectin CRD folds into a β-sandwich shape, having 5 and 6 stranded anti-parallel β-sheets (Yang et al., 2008). The shallow groove formed by the concave S side contains the distinctive galactose-binding site, which is determined by a conserved sequence motif of approximately seven amino acids that are encoded by exons in the CRD-encoding regions of the LGALS loci (Johannes et al., 2018). Each galectin CRD has a unique specificity and stronger affinity for larger glycoconjugates due to weaker regions on each side of the galactose-binding site that may either promote or restrict binding (Newlaczyl & Yu, 2011). At physiological concentrations, galectins are primarily monomeric in solution. However, depending on the concentration or the presence of ligands, several are capable of oligomerase to crosslink glycoconjugate ligands and give rise to their aggregation (Newlaczyl & Yu, 2011). Furthermore, many of the biological functions of galectins, especially when they are exposed to the surface of cells, depend on their multivalency. This enables ligand endocytosis as well as crosslinking of ligands to activate signalling pathways and create cell surface lattices (Dumic et al., 2006).

1.3.1 Galectin-3

Gal-3, a member of the family of lectins that bind β-galactosides, is a 35 kDa protein encoded by the LGALS3 gene located on chromosome 14 in humans. It was initially given the name MAC-2 after being discovered in mouse peritoneal macrophages (Sciacchitano et al., 2018). Later, Gal-3 was demonstrated to be involved in a wide

range of physiological processes including cell–cell and cell–matrix interactions, adhesion, proliferation, apoptosis, pre-mRNA splicing and inflammation.

Being widely found in adults, Gal-3 expression is tissue and time dependent during embryogenesis (Sciacchitano et al., 2018). Gal-3 expression was detected in a wide variety of cells, including epithelial cells of the kidney, heart, lung, breast and prostate, as well as in small intestine epithelial cells and olfactory epithelium (Sciacchitano et al., 2018). Additionally, it was found in the endothelial cells of numerous tissues and organs such as the ductal cells of the salivary glands, pancreas, kidney, heart, eye and fibroblasts. Gal-3 expression in immune cells is also extensively documented; neutrophils, eosinophils, basophils, mast cells, dendritic cells, monocytes and macrophages from various organs were shown to express Gal-3. Furthermore, this protein exhibits abnormal expression in a variety of cancers, including those that affect the thyroid, pancreas, liver, breast, lung, nervous system and prostate (Sciacchitano et al., 2018).

Gal-3 has received the greatest research attention among the other members owing to its broad implications on numerous significant pathologies, as reviewed by Sciacchitano et al. In solution, Gal-3 exists as a monomer. However under certain conditions, for instance when the concentration of Gal-3 is high or ligands are present, it can form dimers or pentamers, being the only galectin able to form pentamers (Sygitowicz et al., 2021). The monomeric form goes through physicochemical changes that broaden the spectrum of its biological functioning, especially the extracellular activity. The multimerization and generation of the Gal-3 lattices are the two most significant processes that manifest in Gal-3 "bioactivation" (Sygitowicz et al., 2021). The oligomerisation in the presence of multivalent carbohydrate ligands is strongly related to the proteins ability of crosslinking glycans on the cell surface. This ability causes transmembrane signalling events to be triggered, which in turn affects a variety of cellular processes (Yang et al., 2008).

1.3.2 Galectin-3 gene and protein structure

Galectin-3 (251 aa) is the only member of the chimeric group, characterised by having a single C-terminal CRD and an amino-terminal polypeptide tail region (Figure 1.5). The C-terminal domain displays a globular structure which contains an Asp-Trp-Gly-Arg anti-death motif (NWGR) and is linked to the N-terminal domain via ~100 aa collagen-like sequence (CLS) domain consisting of repeats of a proline-, glycine-, tyrosine-, and glutamine-rich sequence (PGAY) (Newlaczyl & Yu, 2011). The CRD can specifically recognise and bind β-galactose residues, which

enables Gal-3 to combine with various ligands inside and outside cells to exert biological functions.

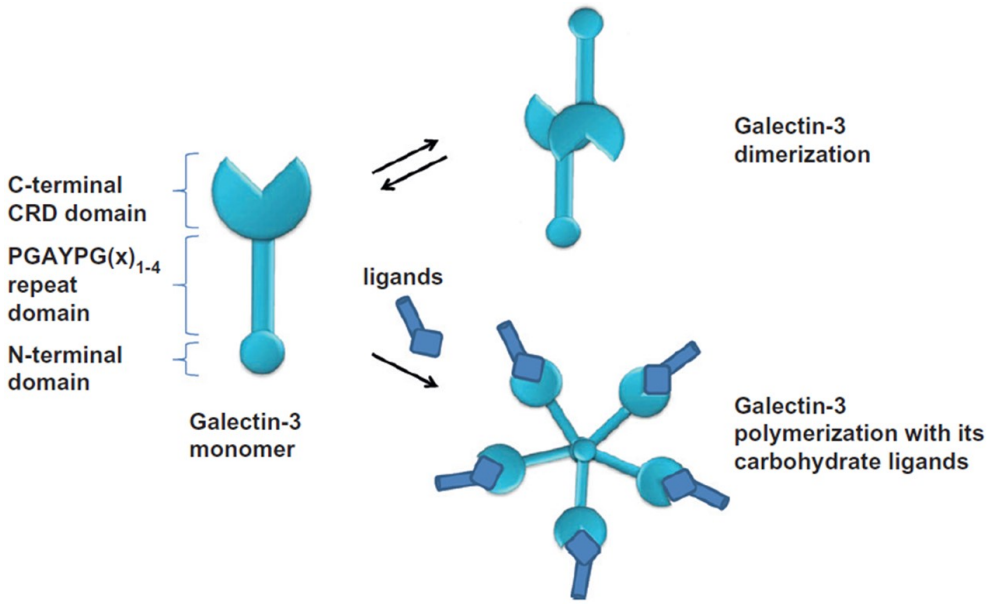

Figure 1.5. Gal-3 protein structure. Schematic representations of the monomeric Gal-3, Gal-3 dimerization through the C-terminal in the absence of ligands and polymerisation through the N-terminal in the presence of carbohydrate binding ligands (Newlaczyl & Yu, 2011).

The N-terminal domain possesses a highly-conserved serine-6 that can be phosphorylated by casein kinase 1 and 2 (CK1/2) (Dumic et al., 2006). This regulation contributes to nuclear translocation and reduced affinity for its ligands. Furthermore, the N-terminal domain was also found to be crucial for the proteins secretion outside of cells. In the absence of ligands, Gal-3 can form a homodimer by dimerizing through the CRD (~130aa) present in the C- terminus whereas it polymerizes into a pentamer via the N-terminal domain when its ligands are present (Newlaczyl & Yu, 2011).

The multi-domain architecture of the protein is compatible with the structure of the LGALS3 gene, made up of six exons and five introns. Most of the 50 untranslated sequences in mRNA are encoded by exon I. The remaining portion of the untranslated sequence, the region in which protein translation begins, and the initial six amino acids, including the first methionine, are all located in exon II. Moreover, exon III codes for the repeated region found in the proteins N-terminal half whereas exons IV, V, and VI encode the C-terminal half (Sciacchitano et al., 2018).

1.3.3 The biological functions of Gal-3

Gal-3 has been found in the nucleus, cytoplasm, on the cell surface and in the extracellular environment, indicating several physiological roles of this protein. Advances in molecular biology, biochemistry, genetics and bioinformatics tools provided the opportunity to study the unknowns about the biological functions of Gal-3, enabling a completely new understanding of the physiological properties of this protein.

1.3.3.1 Apoptosis.

Gal-3 has been discovered to exhibit anti-apoptotic functions in a variety of cell types against a wide range of apoptotic stimuli. The suppression of intrinsic apoptotic pathways is crucial for cell survival. Although the exact mechanisms by which intracellular Gal-3 confers resistance to apoptosis are still unknown, current research indicates that this may involve a functional interplay with other apoptosis regulators in the mitochondria (Yang et al., 2008). This is supported by the findings showing that Gal-3 is more abundant in the mitochondria when the cells are exposed to apoptotic stress (Hsu & Liu, 2002). Moreover, the anti-apoptotic protein Bcl-2 may be implicated in this process, according to the evidence that Gal-3 interacts with Bcl-2 in the mitochondria to carry out its function since the two protein sequences are highly similar. It has been demonstrated that Gal-3 binds to Bcl-2 *in vitro* through its CRD domain (Hsu & Liu, 2002) (Dumic et al., 2006). This anti-apoptotic effect appears to rely on N-terminal serine-6 phosphorylation by CK1 amid apoptotic conditions, where phosphorylation is both required for the export of Gal-3 from the nucleus and anti-apoptotic activities (Yang et al., 2008) (Johannes et al., 2018). As said, the NWGR motif, which is highly conserved in the BH1 domain of Bcl-2 family members, is also present in the CRD of Gal-3. The presence of this motif is highly associated with anti-apoptotic properties. Indeed, a substitution mutation in this region abolishes this function of Gal-3, demonstrating the significance of the NWGR motif (Dumic et al., 2006). In addition, Gal-3 stimulates PI3K/AKT pathway activation, maintaining mitochondrial membrane potential, thereby leading to less caspase-9 and -3 activation and suppression of apoptosis in cancer cells (Dumic et al., 2006). On the other hand, extracellular Gal-3 is associated with apoptotic activities as opposed to its intracellular anti-apoptotic functions.

Furthermore, two recent studies in different disease contexts have revealed the anti-necrotic and anti-necroptotic roles of Gal-3 in knockout (KO) mice via unclear mechanisms (Sygitowicz et al., 2021).

1.3.3.2 Cell Adhesion.

The diverse roles of galectins in controlling cell-cell and cell-matrix adhesion have become increasingly established in several studies (Colin Hughes, 2001) (Argüeso et al., 2015). Galectin expression and distribution, receptor glycosylation, binding valency and the type of receptor determine whether galectins function as negative or positive regulators of cell adhesion (Colin Hughes, 2001).

In different cells and tissues, each galectin exhibits a distinct pattern of expression showing a strictly controlled expression during development. Although most of these proteins are present in the cytoplasm of cells, others are secreted by cells and interact with glycosylated proteins on the cell surface (i.e. cell surface glycans) or in the extracellular matrix. Indeed, Gal-3 was shown to make interactions with a variety of glycoproteins found in the ECM, including fibronectin, collagen IV, elastin, and laminin (Newlaczyl & Yu, 2011) (Argüeso et al., 2015). In addition to these glycoprotein binding partners, Gal-3 was demonstrated to interact with cell-adhesion molecules like integrins and depending on the nature of binding to one or both integrin subunits (carbohydrate-dependent), it can regulate integrin activation and alter binding with external ligands (Sciacchitano et al., 2018). These interactions play a crucial role in regulating proper cellular motility and polarity during tissue formation (Colin Hughes, 2001). Moreover, impaired adhesion has been linked to many disease conditions, including cystic development in branching epithelia, renal tubules, tumour progression, inflammation and cardiomyopathies.

Gal-3 may attach to multivalent glycans to create pentamers, as was previously described. Pentameric Gal-3's multivalency theoretically enables it to serve as a bridge between cells and the extracellular matrix as well as between cells by concurrently attaching to two binding partner glycans. Pentameric Gal-3 may also arrange some cell-surface glycans into lattices (Yang et al., 2008). Desmosomes, adherens junctions, and tight junctions are among the epithelial junctions where Gal-3 is known to be involved (Argüeso et al., 2015).

As previously mentioned, cardiac desmosomes are proteins that provide mechanical connections between cardiomyocytes in IDs, maintaining the structural integrity by conferring adhesive interactions through their IFs. Recent research suggests that DSG-2, a component of desmosomes, interacts with Gal-3 to promote epithelial intercellular adhesion (Jiang et al., 2014). Specifically, Gal-3 has been shown to bind to N-linked β-galactosides on the extracellular domain of DSG-2 in intestinal epithelial cells where Gal-3 deficiency led to the proteasomal degradation of DSG-2 upon internalisation from the plasma membrane (Jiang et al., 2014). It is worth mentioning that Gal-3 binding sites have also been found to co-localize with DSG-2 and DSP-1 in primary squamous carcinomas (Boscher et al., 2012).

Furthermore, recent findings by Cason et al. have demonstrated that upon pharmacological inhibition of Gal-3 in zebrafish embryos, animals displayed abnormal DSP localization in epidermal cells where desmosomes appeared disconnected from the cytoskeletal complex and not regularly distributed (Cason et al., 2021).

1.3.3.3 Wnt/ß-catenin signalling.

As previously mentioned, Gal-3 shuttles between the nucleus and the cytosol in a phosphorylation-dependent manner and was shown to be involved in nuclear splicing of pre-mRNAs and gene expression in the nucleus, redundantly working with Gal-1 as nuclear export and mRNA processing splicing factors (Johannes et al., 2018). In addition, Gal-3 stimulates TCF4 transcriptional activity by binding to the β-catenin/TCF complex and co-localizing with β-catenin in the nucleus (Shimura et al., 2004), which suggests that this protein is required for β-catenin to induce the expression of Wnt responsive genes cyclin D1 and c-myc. This interaction was found to involve the N-terminus and C-terminus of β-catenin and Gal-3 respectively. Later, the same group of researchers focused the attention on GSK3β, suggesting that the interaction between the two molecules can be a key regulator of the Wnt/β-catenin pathway (Shimura et al., 2005).

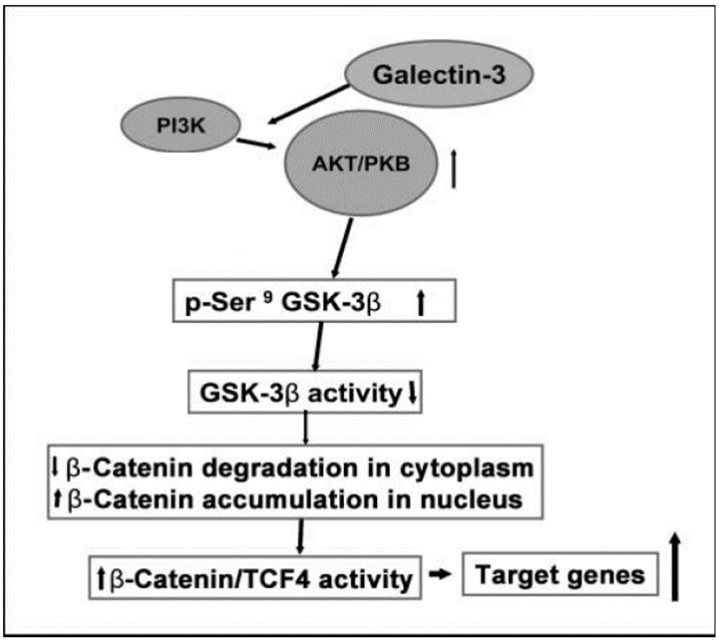

Figure 1.6. Proposed mechanism by which Gal-3 regulates the canonical Wnt signalling in colon cancer cells. Gal-3 increases the phosphorylation of GSK-3β by regulating AKT phosphorylation, thereby increasing the β-catenin activity. TCF4 transcriptional activity is then activated by β-catenin (modified from Song et al., 2009).

Consistent with these findings, Gal-3 was demonstrated to increase β-catenin expression and activate Wnt signalling by regulating GSK-3β activity via the PI3K/AKT pathway in colon cancer cells. In this context, low levels of Gal-3 led to AKT and GSK-3β de-phosphorylation and augmented GSK-3β activity, increasing β-catenin phosphorylation and its subsequent degradation (Song et al., 2009). Furthermore, researchers recently showed that inhibition of Gal-3 in zebrafish embryos by TD139, a drug with high binding affinity for the residues of the CRD domain, is sufficient to suppress the Wnt/β-catenin pathway (Cason et al., 2021).

1.4 Zebrafish as a model organism

The zebrafish (*Danio rerio*) - a tropical freshwater fish - is a cypriniformes teleost that belongs to the lineage of ray-finned fishes, displaying golden and blue horizontal stripes that form during metamorphosis (Figure 1.7). Animal research has been mostly focused on mice, rats and fruit flies. However, alongside more conventional organisms, alternative models are becoming more common. The use of zebrafish in scientific research has become more prevalent in the past decades owing to a number of beneficial traits that make these fish highly practical and effective model organisms.

The great extent of functional conservation in fundamental biological processes shared by mammals and invertebrates indicates that diseases caused by the modification of these processes can be efficiently modelled in flies and worms at the level of molecular genetics. In this context, invertebrate systems offer significant insight into how orthologous human disease genes function in equivalent phenomena. Despite these positive aspects, the potential of invertebrates to mimic human disease is constrained since they fail to have numerous organ systems and structural components that are important in the pathogenesis of human diseases. On the other hand, although mice have many similarities to humans in terms of anatomy, physiology and genetics, they are not manageable on the same scale as in other models since they require a remarkable workforce and infrastructure support. In this regard, attention has lately been drawn to the zebrafish as a genetically tractable vertebrate model organism.

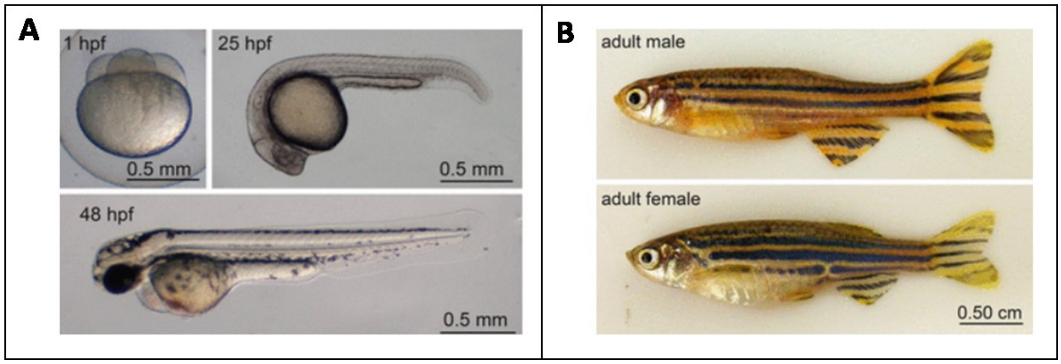

Figure 1.7. Zebrafish embryonic development and adult stage. A) Embryonic stages (4 cell stage- 1hpf, embryo stage- 25hpf, transition into the larval stage- 48dpf. B) Adult male and female. Source: https://ourmarinespecies.com/wpcontent/cache/page_enhanced/ourmarinespecies.com/c-fishes/all-about-zebra-fish/_index.html_gzip (*All about Zebra Fish: Characteristics, Habitat, Employ in Labs and More...*, 2019).

Zebrafish possess high levels of fertility and fast reproductive maturity making the model practical to obtain results in a short period. A zebrafish couple can produce hundreds of eggs per week, which takes around three months to grow into adults. This is particularly advantageous to establish a fish line where plenty of crosses are needed when introducing genetic modifications. Moreover, considering the number of replications required to obtain more accurate results, this time efficiency is a convenient feature when using zebrafish.

Embryonic development outside of the body allows external examination and manipulation. In addition, zebrafish have transparent embryos, which is an extremely useful characteristic, allowing *in vivo* visualisation of several developmental defects and diseases. This feature also possesses a major benefit when combined with reporter transgenic lines that can be used to model a specific pathological condition *in vivo*. A further benefit is that pigmentation can be prevented in zebrafish embryos via chemical treatments, which makes it easy to follow the early embryonic development. Additionally, because the embryos are permeable to a wide range of chemicals, they are suitable for evaluating several toxicological samples or drug candidates.

The zebrafish genome has been fully sequenced, revealing that its genome is quite comparable to the human genome, with at least 70% of human genes having an orthologue in zebrafish. This number rises when only disease-causing genes are considered. In this direction, the zebrafish model is suitable for genetic modifications by adopting forward and reverse genetic approaches such as the CRISPR/Cas9 technology.

However, zebrafish do have several limitations that restrict its practicality. The current dearth of biological resources (e.g. antibodies) with respect to mice is one of them. Another major drawback of this approach concerns the genome duplication that took place during the evolution of teleosts, which led to the emergence of paralogous genes that are not present in mammals, complicating the utilisation of zebrafish to recapitulate certain genetic disorders in humans.

1.4.1 Zebrafish for the study of AC

As discussed above, the zebrafish model has some remarkable benefits that make it powerful as a disease model for a broad range of human pathologies, although bearing less functional and anatomical parallels with humans than its mammalian counterparts (i.e. mouse). These qualities also appear to be significant in recapitulating AC.

The zebrafish organism has become an incredibly powerful organism for understanding cardiac development and disease. The possibility to follow the developmental stages due to optical transparency and external development of zebrafish makes this model animal exceptionally practical in carrying out morphological analyses on the heart even at larval stages. Furthermore, the zebrafish genome can be modified easily and several fluorescent reporter lines (e.g. GFP lines) enable the viewing of cellular and organ-level morphology and function. With regards to the AC disease context, in this way, the intricate and highly debated role of disease-associated signalling pathways (Wnt and Hippo pathways, etc.) and the structural cardiac defects preceded by the desmosome instability can be better determined.

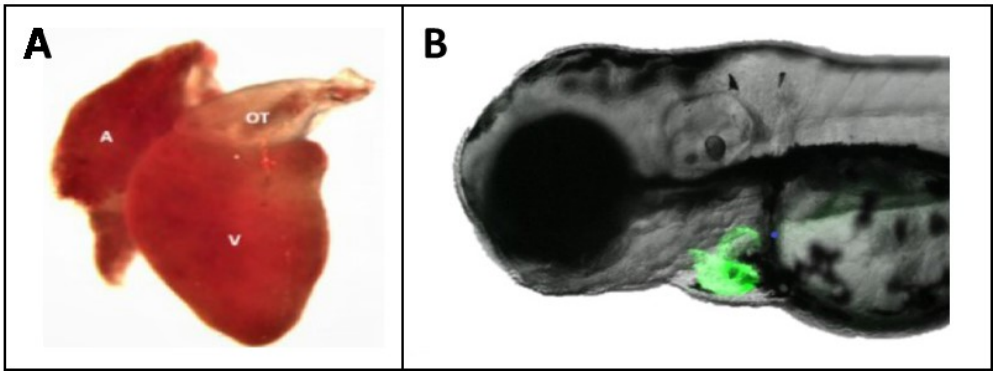

Figure 1.8. The zebrafish heart: adult and larval stage. A) Image of a heart from WT adult zebrafish, with the sponge-like atrium (A), the ventricle (V) and the outflow tract (OT). B) "Green heart" larva (WT) acquired by merging bright-field/fluorescence microscopy.

Unlike the four-chambered hearts of mammals, the zebrafish heart comprises a single atrium and ventricle. However, fish and humans both have a heart that contracts and relaxes in a comparable way at the cellular and molecular levels, including an outflow tract and a sinus venosus that carries the blood into the atrium, the presence of valves and an electrical system that is involved in maintaining the heart rate and rhythm**.** In addition, the heart rate of an adult and 3 dpf (days post-fertilisation) zebrafish is around 120-180 beats per minute (bpm). This feature, in comparison with mice (>300bpm), makes zebrafish a more suitable model to replicate human electrophysiological conditions in AC. Combined with the optical clarity, zebrafish provides a simple estimation of heart rate and rhythm for drug screenings, comparing different lines of WT (wild-type) and mutant fish. Having said that, this can provide insights into the commonly observed arrhythmia and bradycardia episodes in AC.

As was pointed out in the introduction section, AC is highly prevalent in high endurance athletes. It is well established that the disease is exacerbated with increasing physical activity, giving rise to SCD events. Accordingly, the zebrafish model offers the opportunity to conduct training on both larvae and adult fish in methylcellulose and in a fish tank exposed to a water current, respectively. Therefore, the progression of the disease can be followed in resting and training lines, with subsequent histological analysis revealing the pathological features (i.e. fibrosis, adipogenesis, dilation and oedema) in the tissues.

Notably, modelling arrhythmias and cardiac fibrosis associated with AC in zebrafish is perhaps limited due to the regeneration capacity of the zebrafish heart, leading to lack of fibrosis (although some studies do mention zebrafish possessing chronic cardiac fibrosis). Cardiac fibrosis is a significant contributor to the development of AC preceded by tissue remodelling (i.e. fibro-fatty replacement) and arrhythmias. The zebrafish model is still positioned to make significant insights that will have an influence on human health and especially on AC, despite this drawback.

1.4.2 Galectin-3 in Zebrafish

As was discussed before, the zebrafish genome is partly duplicated and has two separate genomic loci for a specific subset of human genes.

Concerning the Gal-3 locus, the zebrafish counterparts are depicted by *lgals3a* (Galectin-3A) and *lgals3b* (Galectin-3B) genes, which are located on chromosomes 13 and 17, respectively. There are currently no scientific articles involving *lgals3b* in any disease context, whereas the effect of reduced *lgals3a* expression on the

development of zebrafish has recently been uncovered by (Chen et al., 2021), where the morpholino line showed defects in various anatomical regions and increased cardiomyocyte apoptosis. Moreover, researchers recently showed that inhibition of Gal-3 expression during zebrafish cardiac development not only dysregulates signalling pathways linked to AC pathogenesis, but also leads to desmosomal instability in the skin and altered distribution of DSP (Cason et al., 2021).

According to our analyses, both *lgals3a* and *lgals3b* are expressed in the zebrafish heart. Scarcity of literature on these orthologues makes it challenging to identify their distinct roles or reason on the molecular mechanisms that they might be involved in. Despite this, in terms of genomic sequence, *lgals3a* exhibits 81.6% similarity to human *lgals3*, making the gene suitable for studying AC in the zebrafish.

2. MATERIALS AND METHODS

2.1 Maintenance of zebrafish lines

All experiments were carried out on fish maintained at the Zebrafish Centre (Facility) of the Vallisneri building – University of Padua. The animals – separated based on their age (larvae, juvenile and adult) and genotype – were kept in a temperature-controlled environment (28.5 °C) with a 12 hrs - 12 hrs dark-light cycle, according to their circadian rhythm in the natural environment.

Zebrafish embryos were maintained in Petri dishes until 7 dpf, manually – then automatically – fed with dry food starting from day 5 and constantly monitored throughout their permanence in the facility's nursery, with water flux control and weekly cleaning of tanks and filters. The pairing of adult individuals (from 3 months onwards) was performed in specific tanks with double bottom that allows the separation of the animals from the newly-produced eggs – an essential precaution due to the natural egg-eating behaviour of *Danio rerio*. The eggs, collected with the help of a strainer, were kept in Petri dishes, cleaned (removal of unfertilized/degraded ones) and placed at the optimal temperature (28.5°C) until 7 dpf.

The anaesthesia or euthanasia of zebrafish embryos was performed with Tricaine (MS222; E10521, Sigma–Aldrich, Milan, Italy), a chemical compound able to inhibit the skeletal muscle activity by blocking the entrance of sodium ions and – thus – the progression of action potentials (0.16 mg/mL for anaesthesia or 0.3 mg/mL for euthanasia). Regarding adult fish, the euthanasia methods (always preceded by the anesthetization) varied according to our purposes (e.g. heart extraction or whole body histological analysis).

Regarding the genotypes, different zebrafish lines were used for our experiments. Wild type lines (Giotto and Tubingen strains), Gal-3 mutant line (lgals3a) and transgenic-reporter lines for the detection of signalling pathway expression and myocardium.

Specifically, two transgenic reporter lines were used in our studies:

• Wnt/β-catenin reporter line *Tg(7xTCF-Xla.Siam:EGFP)*, which expresses the enhanced green fluorescent protein (EGFP) under the control of the Wnt-responsive TCF transcriptional complex (Moro et al., 2013).

• Green heart (GH) line *Tg(tg:EGFP-myl7:EGFP)ia300* in which the GFP is - specifically expressed in the myocardium of the zebrafish heart (under the myosin-7 promoter) (Facchinello et al., 2017).

2.2 *Lgals3a* line

The *lgals3a* mutant line was created by CRISPR-Cas9 technique, with the sgRNA (single-guide RNA) targeting the third exon. The PCR screening of the F0 generation identified, as expected, several types of mutations in the *lgals3a* gene, and the isolation of the germinal ones was obtained by crossing the F0 individuals with wild-type fish. Eventually, after the PCR genotyping of the F1 embryos and sequencing, a frame-shift deletion of 4 bases was selected as the ideal one, being detectable – due to its dimensions – by a classic agarose gel electrophoresis. Following several crosses, *lgals3a* Δ4 -/- line was obtained in homozygosity, which leads to the synthesis of a truncated protein.

2.3 Genotyping of *lgals3a* line

DNA extraction

Embryos at 24-48 hpf (hours-post fertilisation) were placed in 0.5-mL tubes with an anaesthetising concentration of Tricaine - 0.16 mg per mL of fish water (0.5 mM NaH2PO4; 0.5 mM Na2PO4; 1.5 g Instant ocean salts; 2 mg/L Methylene blue) for 2 minutes. After that, the solution was discarded, replaced with 50 µL of the DNA lysis buffer (NaOH 50 µM) and the samples were heated at 85-90 °C for 20 minutes in a thermoblock. At the end of the heating procedure, the tubes were placed at 4°C for 5 more minutes and 5 µL of Tris-HCl 1 M pH 7.5 was added.

The DNA extraction of adult fish was performed with a similar procedure. A small piece of the caudal fin was cut, inserted into 0.5-mL tubes with 50 µl of the lysis buffer (NaOH 50 µM) and heated for 20-25 minutes in the thermoblock. After that, the samples – containing the DNA in solution – were ready for PCR amplification and genotyping.

Genotyping

The *lgals3a* line, carrying a 4bp deletion, was traceable with a classic electrophoresis in a 3.5 % (w/v) agarose – TBE 1X (Tris Borate EDTA) buffer gel.

The following PCR primers were used in the process:

Table 2.1 DNA primers for lgals3a mutant line genotyping.

Gene name	Forward primer (5'-3')	Reverse primer (3'-5')	Product size (bp)
lgals3a	AGGAATGTTTCCTCCAGTACCA	CTTACACGTGCAAACCCATTTA	178

2.4 Western Blotting

Protein extraction

Pools of ten embryos (9 dpf) were treated with 1 mL of deyolking buffer (1/2 Ginzburg Fish Ringer without Calcium: 55 mM NaCl, 1.8 mM KCl, 1.25 mM NaHCO3), shaken for 5 minutes at 1100 rpm to dissolve the yolk sac and centrifuged at 300 g for 30 seconds to pellet the cells. Optionally, two additional wash steps were done by adding 1 mL of wash buffer (110 mM NaCl, 3.5 mM KCl, 2.7 mM CaCl2, 10 mM Tris/Cl pH 8.5), shaking 2 min at 1100 rpm and pelleting as before. Finally, pellets were dissolved in an LDS-sample buffer and incubated for 5 min at 95°C. Extracted proteins were frozen and conserved at -20°C or directly loaded on a gel.

Electrophoresis and Western blot

Proteins were separated on NuPAGE™ 3-8% Tris-Acetate Protein Gels, 1.5 mm, 10-well (Invitrogen, Milan, Italy). The Spectra Multicolor Broad Range Protein Ladder (Thermo Fisher Scientific) was used as a molecular weight marker for protein samples in the 10-260 kDa range.

After the electrophoretic run, proteins were transferred from the gel to a PVDF (polyvinylidene difluoride) Immobilion-P transfer membrane by Mini gel tank apparatus (Invitrogen), following the manufacturer's instructions. The membrane was incubated 1 hour at 4°C in 10% non-fat dry milk in TBS-T (0.1% Tween-20) to saturate, block and avoid non-specific binding of the antibody. Then, it was incubated overnight at 4°C with primary antibody diluted in 5% non-fat dry milk PBST. Secondary antibodies were incubated for 1 hour in 5% non-fat dry milk TBS-T. The signal was detected using an Alliance 9 Mini Chemiluminescence Imaging

System (Uvitec, Cambridge, UK) after incubation with Pierce™ ECL Western Blotting Substrate (Thermo Fisher Scientific).

Band intensities were normalised against Tubulin protein expression. Primary antibodies used for Western blot were: α-Tubulin (mouse, A11126, Invitrogen) diluted 1:1000 in 5% non-fat dry milk TBST; Desmoplakin 1/2 (mouse, 651155, Progen, Heidelberg, Germany) diluted 1:200 in 5% non-fat dry milk TBST. Secondary antibodies used for Western Blot were: Anti-mouse IgG (goat) (H+L)-HRP Conjugate (Bio-Rad, Hercules, CA, USA) diluted 1:2000 in 5% non-fat dry milk TBST.

2.5 Morphological analysis

WT and *lgals3a* mutant embryos (3dpf) were anaesthetised and placed in Petri dishes (or microscope slides) with 2% methyl-cellulose and consequently oriented (lateral view, anterior part on the left) under the dissecting microscope (Leica M165FC). Bright field images were acquired with a Leica DFC7000T camera at 3x - 10x magnification, focusing on the entire embryo and the cardiac region, respectively.

Morphological alterations in the cardiac region, such as dilation, pericardial oedemas and blood effusion, were compared between the two pools (as % on the total embryos), statistically analysed and graphed with GraphPad Prism 7.04. ImageJ software was used to measure cardiac region's dimensions and dilation, with embryos total length and eye-size (generally recognized as developmental indicators) as normalising factors.

Morphological comparison of the hearts was also performed, extracting the organ from adult fish (1-year old) – with tweezers and other dissection instruments – and subsequently acquiring them with aforementioned instrumental settings.

2.6 Heart rate estimate at larval stage

Zebrafish larvae (2, 3 and 5dpf) were anaesthetised in Petri dishes with Tricaine (1 mL in 25 mL of fish water) and placed under the dissecting microscope (Leica M165FC) for subsequent analysis. Heart beats were visually counted – with a single-larva magnification – in 15-second time intervals. Each heart was checked

three times (15 seconds each), and the average result was then multiplied by four, in order to obtain the beats per minute (bpm) statistics.

2.7 RNA isolation and real-time PCR (qRT-PCR)

3 dpf larvae were initially homogenised with glass beads in a tissue-lyser machine (Tissue Lyser II - QIAGEN) for 3 minutes at the maximal speed. Total RNA was separated with the TRIzol - chloroform method (500 and 100 µL, respectively), precipitated with 250 µL of isopropanol and subsequently quantified and checked – for DNA / protein contamination – at the NanoDrop (Thermo Scientific, Milan, Italy) instrument (260/280 260/230 ratios). For gene expression analysis, 1 µg of purified RNA was retro-transcribed – according to sample concentration – with random primers and the M-MLV Reverse Transcriptase RNase H - (Solis BioDyne, 06-21-010000). Real-time quantitative PCR (qPCR) was performed in triplicate (10 µl per well) with the ×5 HOT FIREPol EvaGreen qPCR Mix Plus (Solis BioDyne, Tartu, Estonia) and Light Cycler 480 II (Roche, Monza, Italy).

Table 2.2 Real-time primer sequences for gene expression analysis.

Gene name	Signalling Pathway	Forward primer (5'-3')	Reverse primer (3'-5')	Product size (bp)
gapdh	Housekeeping	GTGGAGTCTACTGGTGTCTTC	GTGCAGGAGGCATTGCTTACA	173
ccnd1	Wnt/β-catenin	CCAACTTCCTCTCGCAAGTC	TGGTCTCTGTGGAGATGTGC	123
myca	Wnt/β-catenin	AGAAAGCTGGAGTCCTCGAC	CTGCTGCAGTGTGTTCAGC	118
ccn2a	Hippo/YAP-TAZ	CTCCCCAAGTAACCGTCGTA	CTACAGCACCGTCCAGACAC	140
ccn2b	Hippo/YAP-TAZ	CCCACAAGAAGACACCTTCC	ATTCGCTCCATTCAGTGGTC	119

Canonical Wnt signalling dysregulation was tested with primers for β-catenin-responsive genes (c-myc, or *myca*, and cyclin D1, or *ccnd1*), while Hippo/YAP-TAZ signalling was checked through the pathway members *ccn2a* and *ccn2b*. The housekeeping gene *gapdh* – coding for the glyceraldehyde-3-phosphate dehydrogenase – was used as a positive control.

2.8 Immunofluorescence analysis

Embryos at 3 dpf were initially fixed in 4% paraformaldehyde (PFA) O/N at 4°C and stored at -20°C in methanol (MeOH) 100%.

In the first part of the procedure, the samples were progressively rehydrated with a series of 5-minute MeOH/PBS washes (75% MeOH 25% PBS, 50% MeOH 50% PBS, 25% MeOH 75% PBS), depigmented with a 2% H2O2 + 3 % KOH bleaching solution and eventually permeabilized – to allow the entrance of the antibodies – by a 7-minute freezing step at -20°C in acetone. At the end of the permeabilization step, embryos were washed with distilled water, then in 1X PBS + 0.5% Triton and subsequently blocked for 30 minutes with a PBDT (PBS 1X + 1% DMSO + 1% BSA + 0.5% Triton X) + 2% goat (or sheep) serum solution, to saturate non-specific binding sites.

To test the cardiac region inflammation, the samples were then incubated for 2 days at 4°C with primary antibodies targeting the L-plastin protein (a leukocyte-expressed protein) in a 1:5000 concentration (1 µL of antibodies in 5 mL of PBDT + goat serum). Unbound primary antibodies were removed with four washes in PBDT (15 minutes x wash), and secondary alkaline phosphatase (AP) conjugated antibodies were subsequently incubated, at 1:1000 concentration, overnight at 4°C. Excess of antibody was washed in PBDT and the fast blue - naphthol staining was eventually performed. This type of staining relies on the hydrolytic nature of the AP enzyme, which removes phosphate groups from the naphthol AS-MX substrate and produces a coloured (blue) precipitate after the coupling between the newly produced phenolic compound and the fast blue salts. The fast blue staining allows to detect a signal both in the bright field – where the coloured precipitate can be used to check the efficacy of antibodies incubation – and in the fluorescent spectrum, with the emission of a far-red signal that identifies, specifically, the localization of the protein of interest.

After the removal of the staining solution, the samples – ready for the acquisition – were then either conserved in the dark at 4°C in PBS 1X or directly mounted on glass slides with glycerol. Fast blue fluorescent signal was detected at the confocal microscope (Leica TCS SP5), and Z-stack images of the cardiac region were subsequently analysed with the ImageJ software.

2.9 Acridine Orange staining

Dechorionated embryos at 3 dpf were incubated in 15 µg/mL acridine orange in fish water for 30 minutes at RT. Embryos were then washed three times with fish water at RT (or PBS/PBT) for 5 minutes. The fluorescent signal was observed under the fluorescent microscope *in vivo* with Tricaine in Methylcellulose 2%.

2.10 Mortality rate assay

To study the mortality rate, zebrafish larvae were monitored for 30 days starting from 3 dpf, counting the number of deaths for each condition (wild-type, mutant, treated larvae) on a daily basis, and eventually constructing a survival curve with the collected data.

2.11 Statistical analysis

Graph Pad Prism V7.0 software was used for the statistical analyses. Pairwise comparisons of two samples were performed with the unpaired t-test method (parametric) or Mann-Whitney test (non-parametric), while multiple comparison analysis was carried out with the parametric analysis of variance (ANOVA), according to the assumption of normality. Survival rates analyses were instead performed with the Log-Rank (Mantel -Cox) method, a non-parametric test which is commonly used for these kinds of experiments. In the charts, error bars display standard errors of the mean. Asterisks indicate significant differences from controls. Correspondence between asterisks and significance levels is indicated in the figure's captions.

3. RESULTS

3.1 Genotyping

To ensure the accuracy and reliability of the findings, the genomes of lgals3a mutant zebrafish lines were continuously examined. As mentioned in the Materials and Methods section, the *lgals3a* gene was analysed by PCR amplification followed by agarose gel electrophoresis in 3.5% (p/v) agarose (Figure 3.1), providing the identification of the 4-nt deletion that defines this mutant line.

Considering this, we distinguished the genotypes by employing gel electrophoresis, representing WT (*lgals3a* Δ4 +/+), heterozygous *lgals3a* +/- and homozygous *lgals3a* -/- individuals in the columns 1, 2 and 3 respectively, along with the marker. The lgals3a -/- profile displays a single band, lighter than the WT band, running faster in the gel and indicating the deletions (in both alleles), whereas the *lgals3a* +/- profile can be recognised having both WT and 4-bp deletion bands in the gel (Figure 3.1).

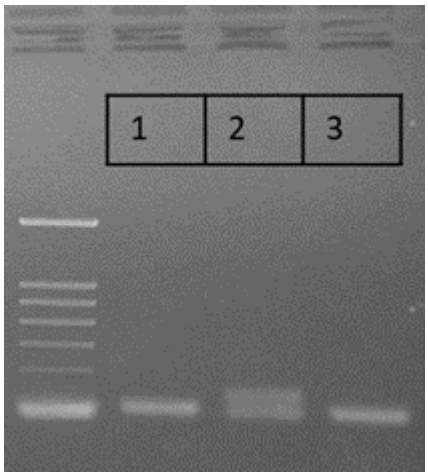

Figure 3.1. Genotyping of the *lgals3a* gene. Analysis by agarose gel electrophoresis of DNA extracted from zebrafish (obtained by inter-crossing *lgals3a* heterozygotes) and amplified by PCR. Column 1) WT genotype, 2) heterozygous +/- genotype, 3) homozygous -/- genotype.

The PCR products of the WT and homozygous samples were sequenced by Sanger method to confirm the electrophoresis results, since the 4-bp deletion cannot be distinguished with certainty. Electropherograms demonstrated the missing CACC sequence in the targeted region of homozygotes (Figure 3.2, panel A) whereas the

CACC sequence is present in WT (Figure 3.2, panel B). The *lgals3b* line was disregarded due to fertility issues.

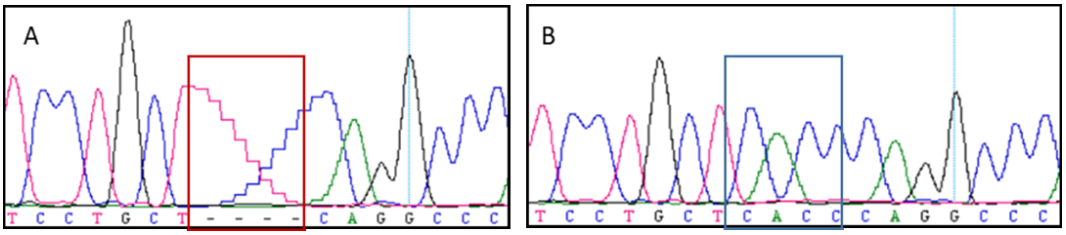

Figure 3.2. Genotyping of the *lgals3a* gene. Electropherograms obtained by Sanger sequencing of the *lgals3a* gene. Homozygotes have the CACC sequence deletion in both alleles (A, red box) while wild-type individuals have the CACC sequence in both alleles (B, blue box).

3.2 *Lgals3a* mRNA expression

The WT and *lgals3a* -/- lines were raised to 3 dpf and the mRNA expression level of the gene was detected using qRT-PCR.

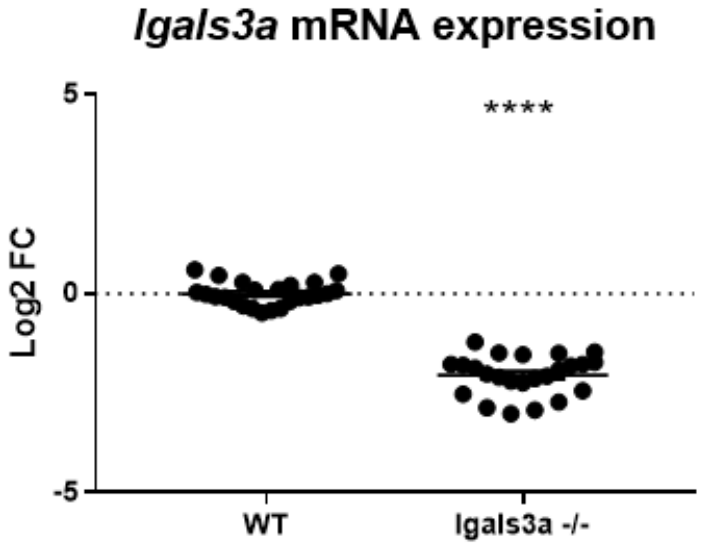

Figure 3.3. Gene expression analysis of *lgals3a* in *lgals3a* -/- zebrafish. In the y-axis, the log2FC (log Fold Change, effect size estimate) statistics indicate the level of mRNA change compared to the (WT) control. (**** p-value < 0.0001) Test: Unpaired t-test.

Our results indicate a significant decrease in the expression of *lgals3a* mRNA in comparison to the WT zebrafish, confirming the suppression of *lgals3a* expression by approximately 50% (Figure 3.3).

3.3 Desmoplakin protein expression

It was demonstrated that Gal-3 deficiency can alter the desmosome integrity in the skin (Cason et al., 2021) and that Gal-3 co-localises with DSP in primary squamous carcinomas (Boscher et al., 2012) (i.e. Dsp mutations are common in AC patients). Therefore, the protein expression of Dsp was analysed in *lgals3a* -/- mutants to investigate whether Gal-3 deficiency leads to lower expression of Dsp. Double heterozygous (DH) *dsp* zebrafish line was also considered as positive control to have an idea about the extent of alteration with respect to Dsp-deficient zebrafish.

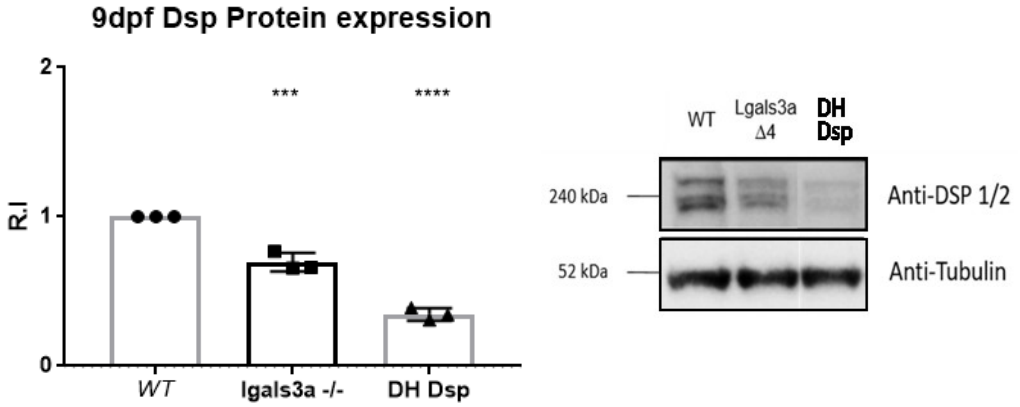

Figure 3.4 Western blotting analysis of Dsp protein expression and the corresponding quantification. The histogram on the left shows the ratio of Dsp to tubulin in the different lines. The image on the right illustrates the PVDF obtained by Western blot where the band intensities were normalised against tubulin protein expression. *** p-value < 0.001, **** p-value < 0.0001. Test: Ordinary one-way ANOVA with multiple comparisons.

The image in Figure 3.4 illustrates that WT larvae exhibit three bands at ~240kDa corresponding to the two Dspb isoforms and Dspa single isoform. As DH Dsp larvae possess lower levels of Dsp, the three bands are present with lower intensities. Homozygous *lgals3a* -/- larvae also exhibit the bands with lower intensity but not as low as in the DH Dsp line (Figure 3.4), as it could be expected.

To quantify the expression of Dsp, for each sample, the intensity of Dsp was compared with the intensity of β-tubulin (housekeeping protein) band for normalisation. Our results demonstrate that Dsp protein expression is significantly lower in *lgals3a* -/- and DH Dsp lines compared to WT, being the lowest in DH Dsp zebrafish (Figure 3.4).

It was not possible to analyse Gal-3 protein expression by Western blotting due to the unavailability of a working antibody for zebrafish.

3.4 Wnt/β-catenin signalling suppression

Prior studies have shown an association between Gal-3 and GSK-3β activity/Wnt signalling regulation, with abnormal GSK-3β distribution and Wnt suppression appearing to be crucial in disease progression (Chelko et al., 2016). In order to investigate this, the Wnt/β-catenin pathway was analysed by the quantification of signal intensity in Wnt responsive GFP transgenic 3dpf embryos (*Tg(7xTCF-Xla.Siam:GFP)*). The corresponding results (i.e. reporter intensities) are normalised to the area of the considered region after the elimination of the background noise.

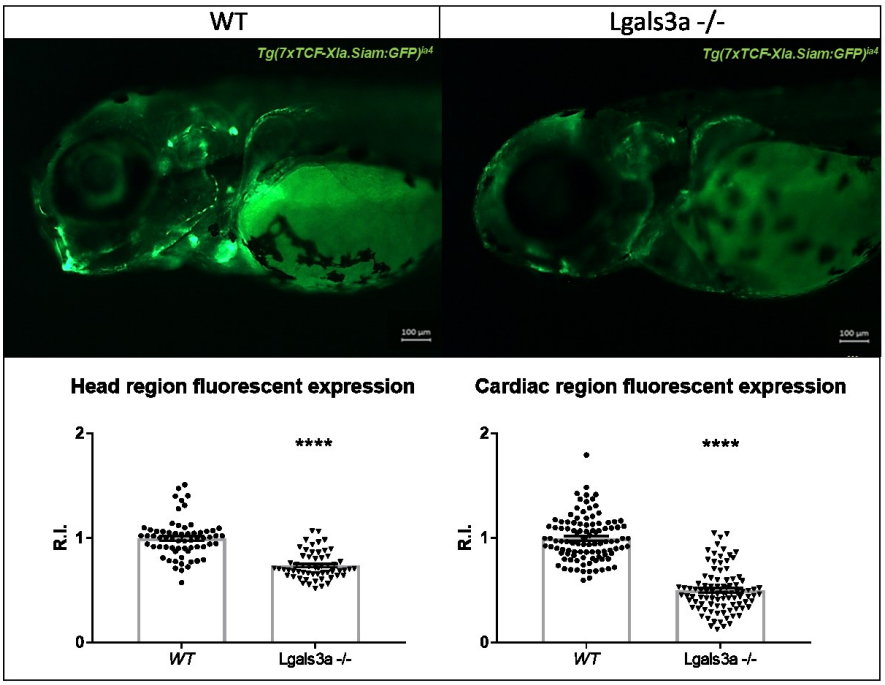

Figure 3.5. Canonical Wnt signalling quantification in WT and *lgals3a* -/- larvae at 3 dpf. Top images: Wnt/β-catenin responsive GFP fluorescent signal in 3 dpf transgenic embryos. All samples are in lateral view, anterior to the left. Bottom plots: scatter plots of fluorescence intensities in the different pools. **** p-value < 0.0001. Test: Mann-Whitney test. R.I. = relative intensity.

Homozygous *lgals3a* -/- displayed significantly reduced Wnt signalling compared to their WT counterparts, indicated by the fluorescent signal in the cardiac and head region (Figure 3.5). Considering the images, both the oral region and the valves of the zebrafish heart - Wnt-expressing areas - were clearly presenting a stronger signal in WT controls compared to *lgals3a* -/-. Quantification of this difference in the Wnt-responsive signal confirmed the suppression of the Wnt signalling in *lgals3a* -/- larvae, with a high statistical confidence in both head and cardiac regions (p-value < 0.0001).

3.5 Wnt target genes expressions

The level of activation of the Wnt canonical signalling was also assessed through qRT-PCR on the messenger RNA transcripts (mRNAs) of two of the key β-catenin responsive genes, c-myc (*myca*) and cyclinD1 (*ccnd1*).

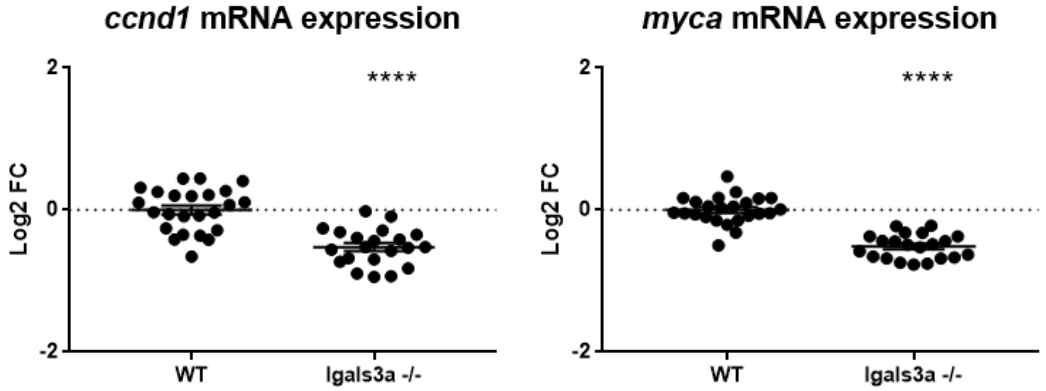

Figure 3.6. Gene expression analysis of *myca* and *ccnd1* in WT and *lgals3a* -/- larvae at 3 dpf. In the y-axis, the log2FC (log Fold Change, effect size estimate) statistics indicate the level of mRNA change compared to the (WT) control. **** p-value < 0.0001. Test: Unpaired t-test.

Consistent with previous analysis on transgenic embryos, both mRNA levels are decreased in the mutant line, with a high level of significance (Figure 3.6).

3.6 YAP-TAZ target genes expressions

Hippo/YAP-TAZ pathway is another important pathway not only because of its relevance for cardiac development and function but also considering the adipogenic roles possessed by its effectors YAP and TAZ. Accordingly, YAP-TAZ-dependent transcriptional activation was evaluated by qRT-PCR on the mRNAs of zebrafish orthologues (connective tissue growth factor (CTGF) or cellular communication network 2 (CCN2) *ccn2a* and *ccn2b*, two targets of Hippo transducers YAP-TAZ.

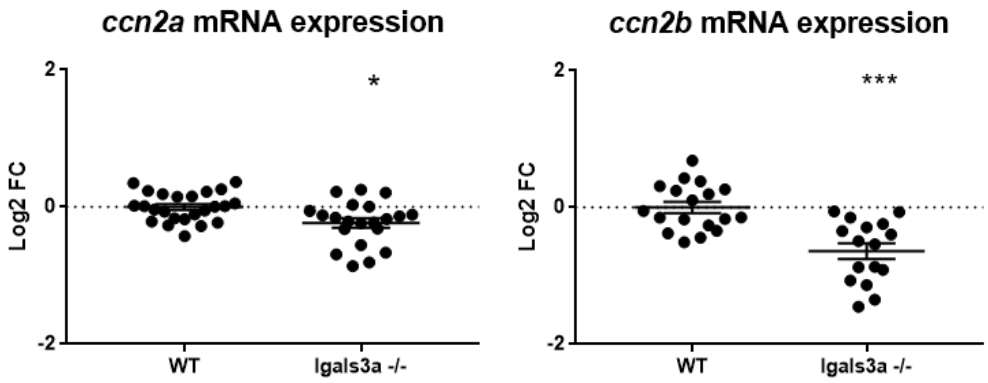

Figure 3.7. Gene expression analysis of *ccn2a* and *ccn2b* in WT and *lgals3a* -/- larvae at 3 dpf. In the y-axis, the log2FC (log Fold Change, effect size estimate) statistics indicate the level of mRNA change compared to the (WT) control. * p-value < 0.05, *** p-value < 0.001. Test: Unpaired t-test.

As shown by Figure 3.6, the expression of the YAP-targeted gene *ccn2a* was mildly downregulated in mutants at 3 dpf while, at the same developmental stage, *ccn2b* was strongly downregulated compared with the WT line.

3.7 Morphological analysis

Morphological alterations were assessed comparing zebrafish mutants with WT controls at 3 dpf. Among these alterations were cardiac dilation, oedemas and blood effusions in mutant larvae. Moreover, developmental defects were also evaluated, taking into consideration the eye size and body length as indicators of zebrafish development. Cardiac area/length and eye area/length ratios were calculated for the *lgals3a* -/- line and normalised to the mean corresponding ratios for the WT.

Cardiac region alterations can be appreciated in Figure 3.8, where 3 dpf *lgals3a* -/- and WT zebrafish are illustrated. Overt defects in the cardiac region of the mutant larvae was observed with a significant dilation of the cardiac region, pericardial oedema and blood effusion. These changes were not evident in WT larvae. Accordingly, the area of the cardiac region was found to be ~20% larger compared to WT controls (Figure 3.8). Furthermore, the heart was distinguishable from the surrounding cardiac region in mutant larvae with respect to the WT animals possessing a more uniform and organised structure.

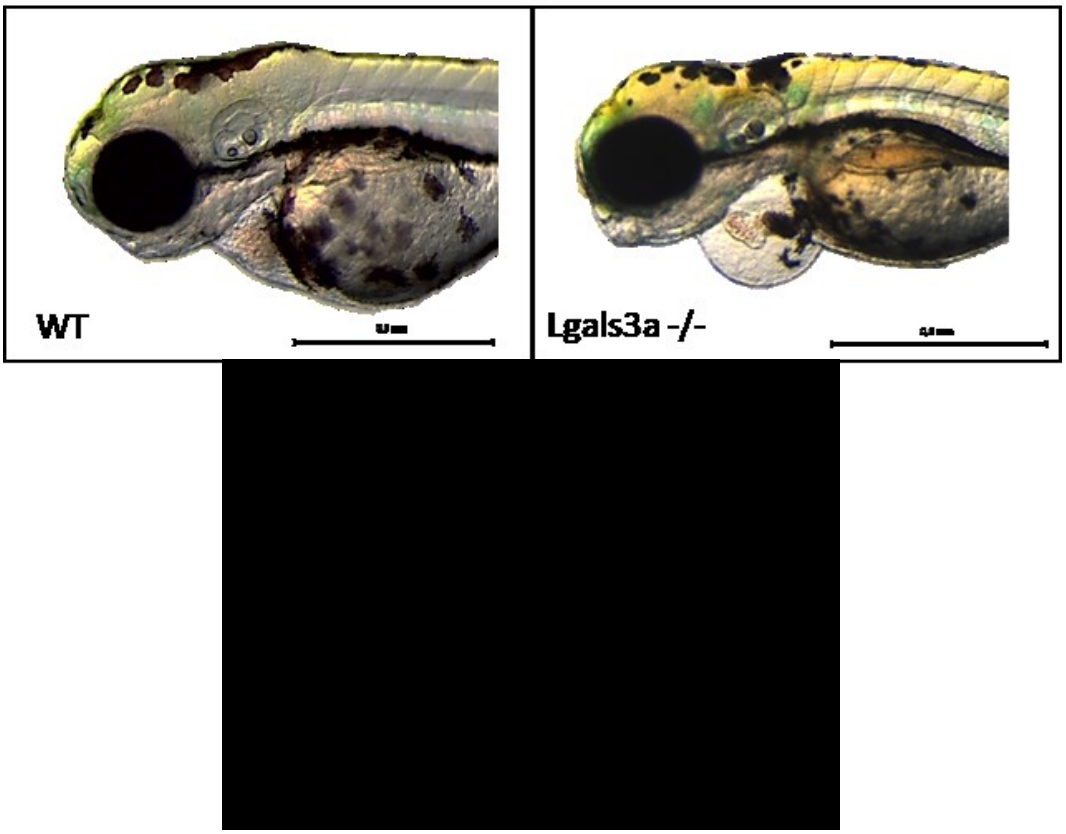

Figure 3.8. Morphological analysis of the cardiac region at 3 dpf. The heart area of the *lgals3a* -/- larvae was compared with WT larvae, and morphological alterations were assessed. In the plot, asterisks indicate the level of significance (**** p-value < 0.0001); R.R. is the relative ratio, indicating that each value – divided by the length of the embryo – was normalised to the WT reference pool. Test: Mann-Whitney test.

Upon examination of the morphological alterations at the level of the cardiac region, 35% of *lgals3a* -/- larvae showed at least one cardiac morphological abnormality, whereas this number was 10% for the WT zebrafish (Figure 3.9). These results are in line with the area analysis on the cardiac region, clearly indicating a dilation in the cardiac region with a high significance.

.

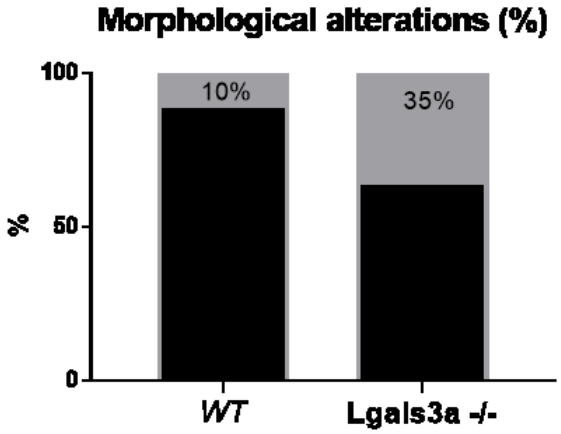

Figure 3.9. Percentage of cardiac morphological alterations found in WT and *lgals3a* -/- larvae at 3 dpf. The number of animals which presented at least one morphological feature was quantified (%). Grey columns represent the amount of altered larvae in the considered pools.

Developmental defects were analysed by comparing the body length and eye area - along with cardiac region area- in *lgals3a* -/- and WT larvae. Figure 3.10 illustrates a significant reduction in both parameters for the mutant larvae with respect to WT animals.

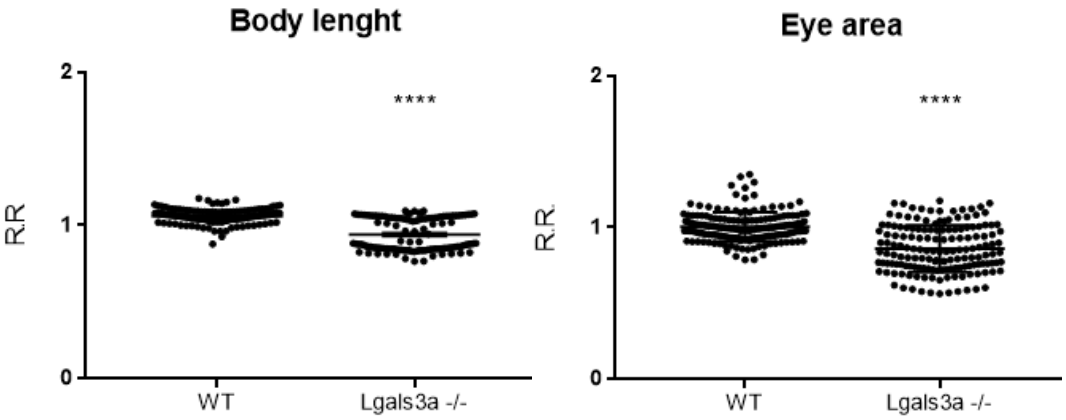

Figure 3.10. Morphological analysis of body length and eye area of *lgals3a* -/- larvae compared with WT larvae at 3 dpf. In the plots, asterisks indicate the level(s) of significance (**** p-value < 0.0001); R.R. is the relative ratio, indicating that each value – divided by the length of the embryo – was normalised to the WT reference pool. Test: Mann-Whitney test.

3.8 Heart rate estimation

Cardiac arrhythmia is another feature of AC. To examine possible variations between the WT and the mutant larvae in terms of number of bpm, each larva's heart rate was counted three times over a period of 15 seconds - as previously described - to determine the mean bpm values. To evaluate potential changes in the pattern of variation of this specific cardiac phenotype, this assessment was performed in an identical fashion, at various developmental stages. The findings are illustrated in Figure 3.11.

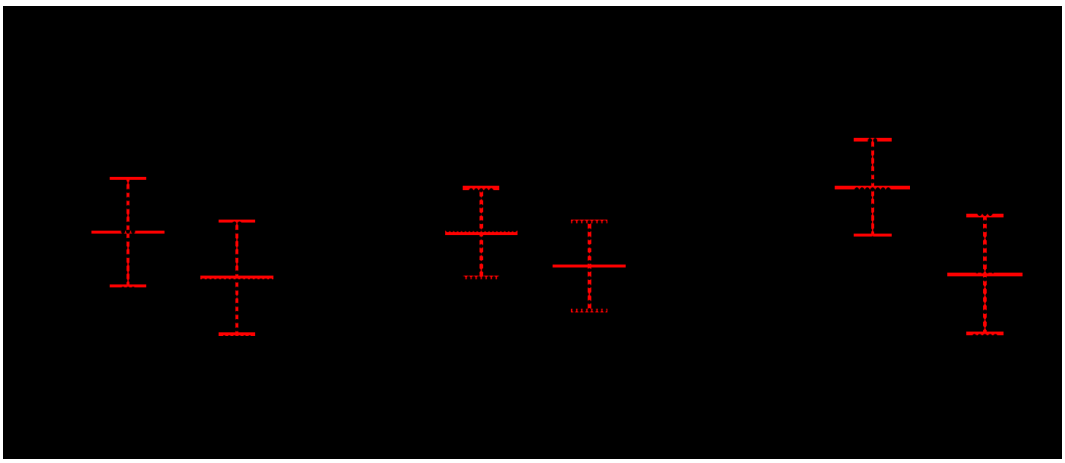

Figure 3.11. Heart rate estimation (bpm) in *lgals3a* -/- and WT larvae. In the plots, asterisks indicate the level(s) of significance (**** p-value < 0.0001); Test: Mann-Whitney test.

The resulting statistics highlight the finding that *lgals3a* mutants displayed a bradycardia (slow heart rate) phenotype, which began to manifest at 2 dpf and persisted with amplified differences (considering a 2-5 dpf interval) in the following days. Therefore, a trend of bradycardia was maintained throughout the analysis, with a high level of significance. Particularly, a larger difference is apparent between the two groups at 5 dpf, when the heart bpm is reduced by 40 beats on average in mutant larvae. This difference is 24 bpm and 15 bpm at 2 dpf and 3 dpf, respectively.

3.9 Heart chambers dilation

Furthering the precision and relevance of the prior morphological characterisation, Green Heart (GH) transgenic embryos (*Tg(tg:EGFP-myl7:EGFP)ia300*) were utilised to analyse the level of dilation (a feature of AC) in the two heart chambers of the mutated zebrafish, independently of the cardiac region itself. Thereby, the

overall size of the chambers was quantified according to the merged fluorescence and bright field images (Figure 3.12).

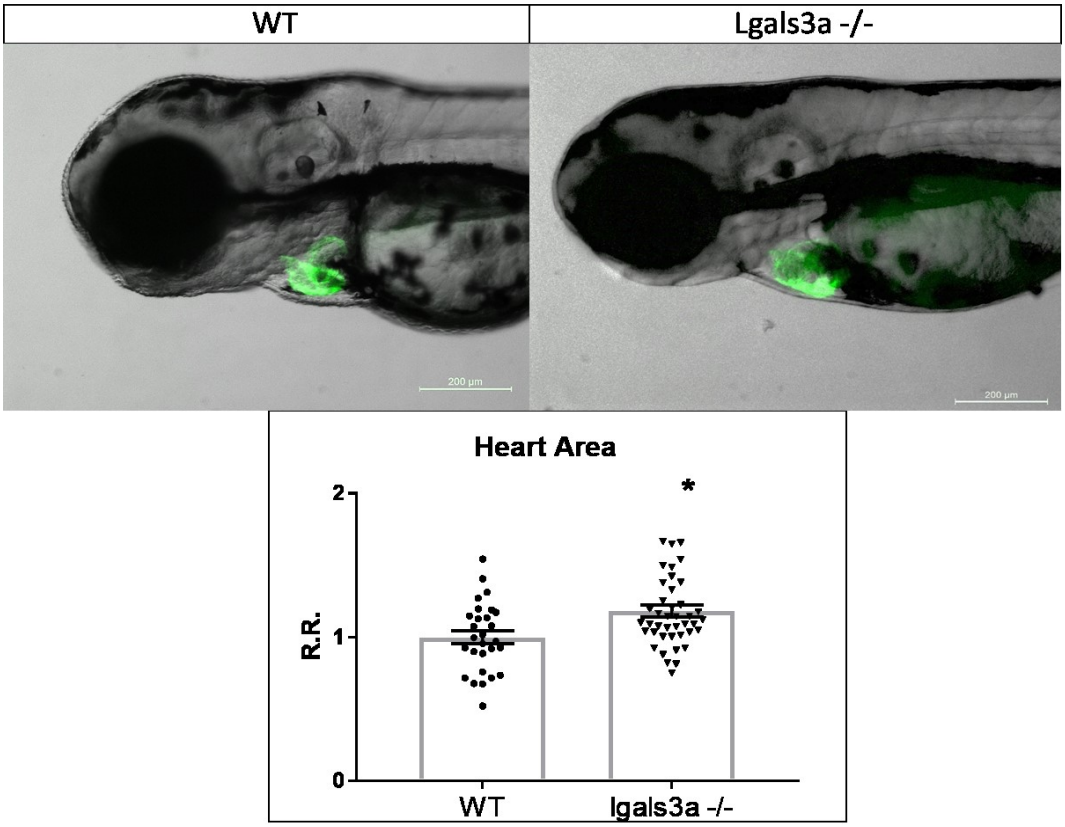

Figure 3.12. Heart chambers dilation in *lgals3a* -/- and WT larvae at 3 dpf. Heart dilation was both qualitatively and quantitatively analysed; all embryos are in lateral view-anterior to the left. * p-value < 0.05. Test: Mann-Whitney test. R.R. = relative ratio.

Close inspection of the images alone has revealed an enlargement in the hearts of *lgals3a* -/- zebrafish, with a greater volume/area in comparison to the WT condition. In fact, the two chambers of the zebrafish heart in the mutant line are no longer distinguishable -underlining the extent of the dilation-, while in the WT, the ventricle (bottom, anterior) and the atrium (top, posterior) are clearly visible.

Following statistical analysis, this dilation was shown to be significant and consistent with the cardiac region analysis, with a mean dilation of approximately 20% when compared to the WT line (Figure 3.12).

To extend our understanding of the level of dilation, it was of interest to assess adult hearts of the two genotypes. Accordingly, our investigations proceeded with the extraction of adult hearts from 1-year-old zebrafish. Due to the relevance of the ventricle in the manifestation of AC, and because of the fragility of the atrium during extraction, atria were unregarded in this process, while ventricles were

carefully isolated. Therefore, the adult heart analysis consisted of a focus on the ventricle in which the ventricular areas were quantified (Figure 3.13).

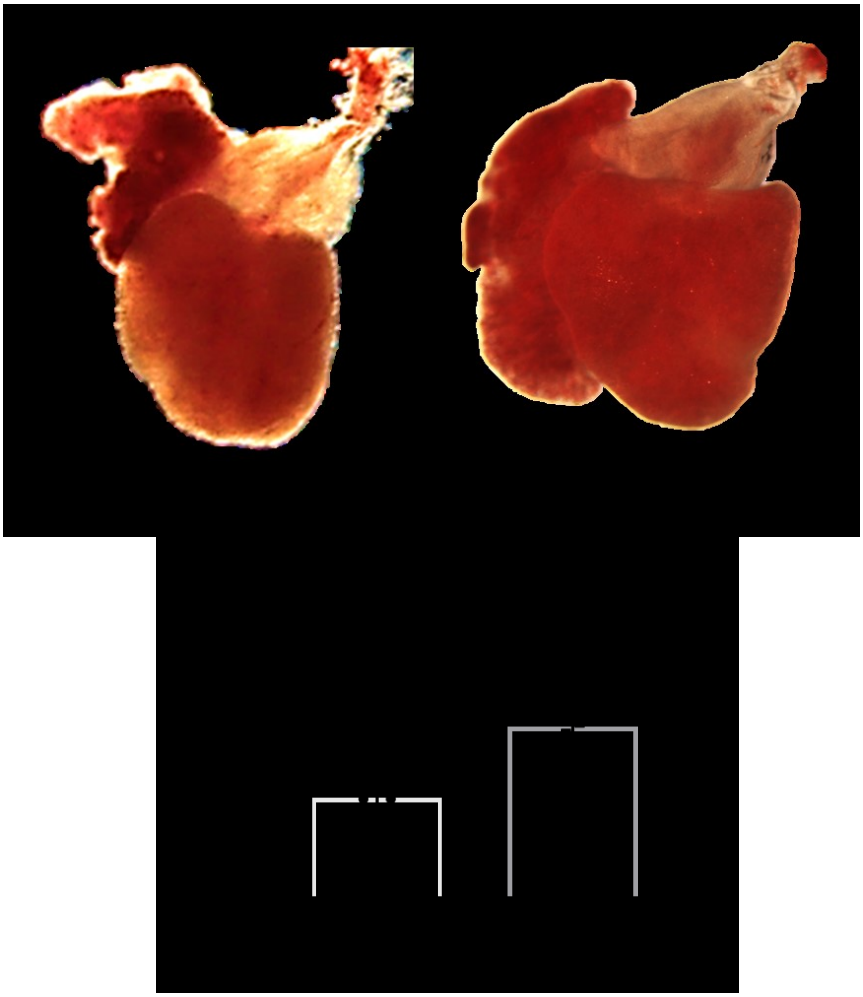

Figure 3.13. Ventricle area comparison in 1-year-old zebrafish. Mutant and WT zebrafish hearts were compared based on their ventricle area, quantifying the ventricular dilation in the *lgals3a* -/- line. * p-value < 0.05. Test: Unpaired t-test. R.R = relative ratio.

Our findings demonstrate that the mutant heart possessed an overt ventricle dilation compared to the WT counterparts, with a more than 2-fold increase (~ 70%) of the ventricle area (Figure 3.13).

3.10 Immunofluorescence analysis

The pathophysiology of AC has been linked to cardiomyocyte inflammation (Yuan et al., 2021). Therefore, to determine the level of inflammation in WT and mutant zebrafish - considering the role of Gal-3 on it-, the expression of L-plastin, a

leukocyte-specific marker (revealing neutrophils and macrophages), was analysed by performing an immunofluorescence experiment on 3 dpf larvae as a preliminary measure (Figure 3.14).

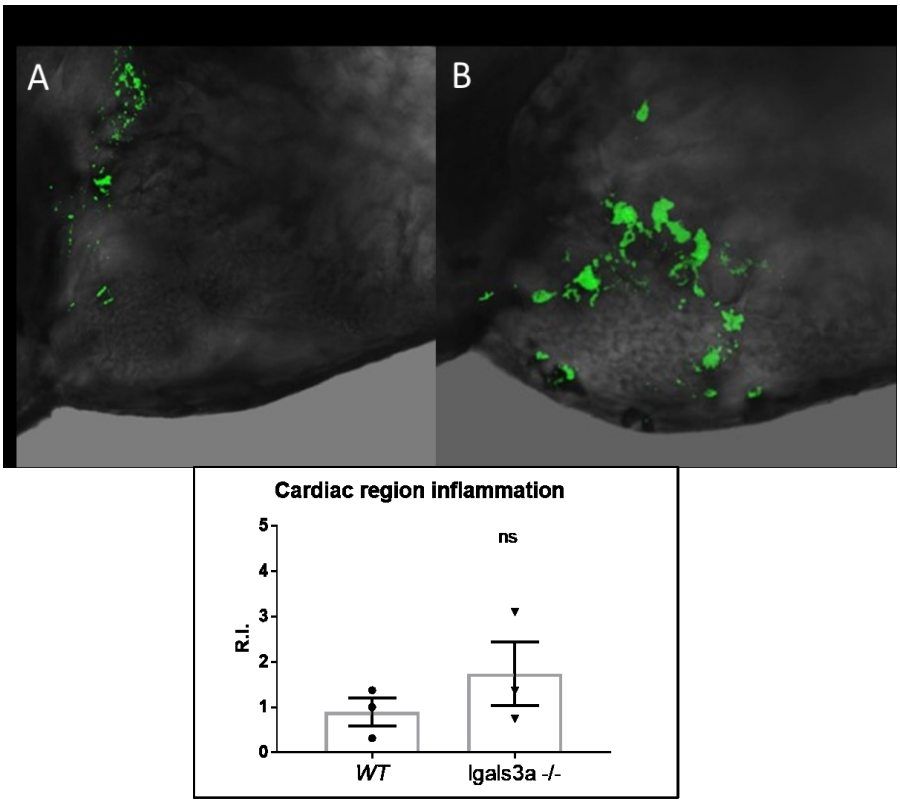

Figure 3.14. Immunofluorescence analysis on WT and *lgals3a* -/- larvae at 3 dpf. Fluorescent images of two genotypes were quantified in terms of relative intensity (R.I.) - background intensity was subtracted and normalised. Larvae are in lateral view, anterior to the left. P-value > 0.05 (not significant (ns). Test: Unpaired t-test.

The fluorescence expression, compared between the two conditions, was not significantly different (Figure 3.14). Although the leukocyte-specific signal did not statistically differ, the mean of the fluorescence signal in the mutant was higher than the WT one, with almost two out of three mutant larvae that presented a higher intensity with respect to the WT group, suggesting possible differences between these two pools but, to draw solid conclusions and obtain significant results, the sample size should be increased.

3.11 Acridine Orange staining

The developmental defects in the heart can be due to numerous mechanisms such as increased cell death and/or reduced cell proliferation. Moreover, cardiac regions in which cardiomyocyte loss tends to occur are often surrounded by fibro-fatty

replacement, immune cell infiltration and inflammation (Meraviglia et al., 2021). To assess cell death as a possible mechanism, we analysed the level of cell death through acridine orange staining in WT and mutant larvae at 3 dpf (Figure 3.15).

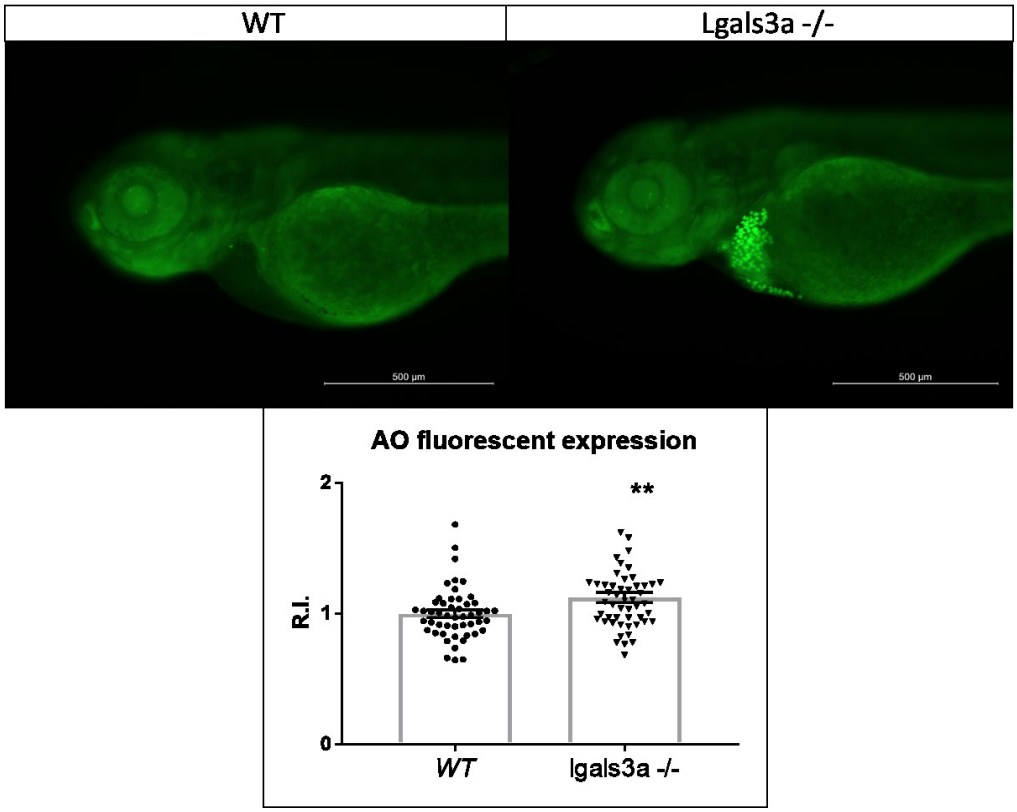

Figure 3.15 Evaluation of cell death by Acridine Orange (AO) staining at 3 dpf. AO green fluorescence intensity was quantified comparing the WT and *lgals3a* -/- pools. All samples are in lateral view, anterior to the left. ** p-value < 0.01. Test: Mann-Whitney test. R.I. = relative intensity.

Acridine orange staining of living larvae revealed increased staining of cardiac cells in the mutant fish compared to WT (Figure 3.15).

3.12 Survival rate analysis

The influence of Wnt pathway suppression, heart dilation, cell death, bradycardia and other morphological changes on the lifetime of the mutant zebrafish was evaluated for 30 days. Therefore, WT and *lgals3a* -/- pools were monitored, counting the number of deaths every day, to assess the survival rate of each genotypic condition. Each line was reared under the same conditions to limit the environmental variability.

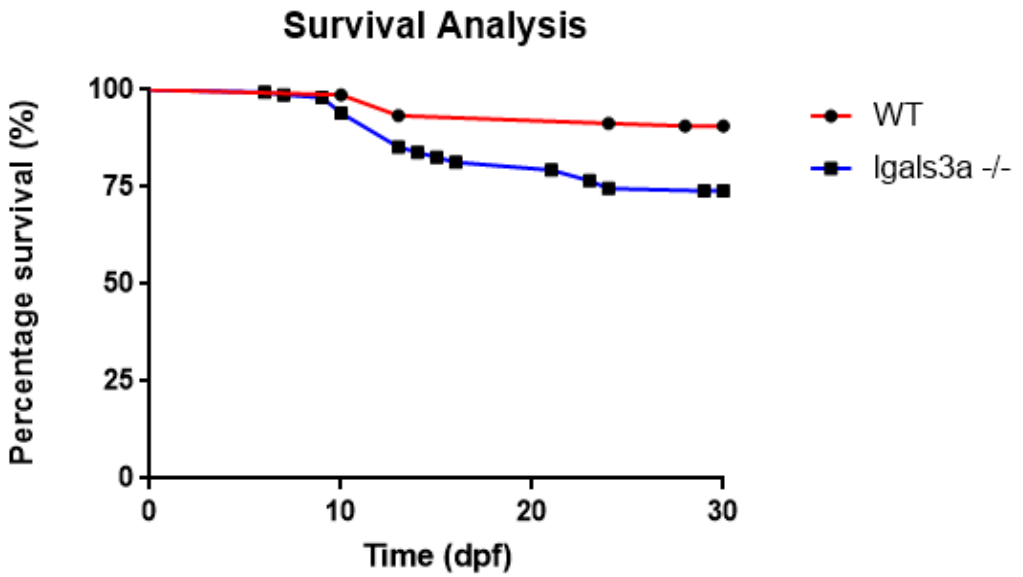

Figure 3.16. Survival analysis of WT versus *lgals3a* -/- larvae. Survival percentages were determined based on counting the number of deaths on a daily basis. Test: Log -Rank (Mantel – Cox) test.

The results (Figure 3.16) indicate that the deaths in larvae tended to emerge at about 9–10 dpf, regardless of the genotype. Importantly, it is evident that from that point on, the curves of the various genotypes diverge, with the slopes and amplitudes representing the consequences linked to each distinct pool. Specifically, a spike in the fatalities was encountered starting from day 10, up until day 13, giving rise to a drop in the percentage of alive mutant zebrafish by 15%. In the following days, this decrease appeared to be more gradual, also in the case of the WT pool. The result obtained from 30 days of examination shows the survival proportions to be 90.7% and 74% in the WT and mutant pools respectively, with a high level of statistical significance. Overall, the life expectancy of *lgals3a* -/- zebrafish was ~17% lower than that of the WT line.

4. DISCUSSION

Arrhythmogenic cardiomyopathy is a complex disease arising from the involvement of multiple pathological processes, acting both individually and collectively, also due to the interplay of fundamental signalling pathways. These concomitant phenomena provoke the distinctive phenotypic feature of AC, the fibro-fatty substitution of the myocardium. Accordingly, AC research requires a detailed genetic and molecular examination of disease-related mechanisms, evaluation of structural myocardial abnormalities and the assessment of electrophysiological features of the heart. Our study, inspired by the recent findings of Cason et al., underlines the possible involvement of Gal-3 in the manifestation of AC – as suggested by a functional KO of Gal-3 in zebrafish - and highlights *Danio rerio* as a potent animal model for AC research, especially in the early phase of the disease.

First off, the functional KO model of *lgals3a* is currently awaiting full validation due to the unavailability of a functional antibody for Gal-3**.** However, our results show that the mRNA level of *lgals3a* is depleted by ~50% (Figure 3.3), suggesting the presence of some mRNA that may lead to the production of a truncated protein. It is an established concept that mRNAs with premature termination codons, as in our case, are targeted for degradation by nonsense mediated mRNA decay. However, those mRNAs that escape from degradation are expected to be translated into truncated proteins. Although there are cases in which truncated proteins can partly function and interfere with the desired outcome (depending on the eliminated region), the C-terminal truncated (i.e. CRD region) Gal-3A in zebrafish should leave the protein incapable of proper functioning since the missing portion is critical for its binding activities. Therefore, presumably, the 4-nt deletion leads to a loss of function effect since the conserved CRD domain is no longer present.

Focusing on the signalling pathways that are associated with AC, the expression of the Wnt/β-catenin signalling was evaluated by qRT-PCR and *in vivo* fluorescent analysis. In both cases, a significant suppression of the pathway was observed in mutant larvae as evidenced by the downregulation of Wnt signalling in GFP transgenic fish and Wnt target genes. Our results are consistent with previous findings on the involvement of Gal-3 in the regulation of Wnt/β-catenin pathway, where Gal-3 deficiency suppressed Wnt signalling and target gene expression by increasing the activity of GSK-3β through PI3K/AKT pathway dysregulation (Song et al., 2009). The central role of GSK-3β in AC has been covered by Chelko et al. Apart from these direct effects, considering the adhesive role of Gal-3 at the level of desmosomes (Cason et al., 2021), it can be postulated that downregulating this protein not only leads to the weakening of intercellular junctions at the IDs, but

triggers the release of JUP (due to desmosome instability) from the cell surface, thus suppressing the canonical Wnt/β-catenin signal by competing with β-catenin, in the nucleus, for TCF/LEF transcription factor binding. This is expected to induce adipogenesis, fibrogenesis and apoptosis (i.e. myocardial fibro-fatty replacement).

Moreover, it is well established that components of IDs other than desmosomes and cardiac ECM components are strongly connected to one another and act as an orchestra of molecules to maintain the structural integrity and electrophysiological properties of a healthy heart (Song & Zhang, 2020). In this context, recent findings by Cason et al., and other studies suggest a potent role played by Gal-3 in regulating desmosome stability and function by interacting with DSP and DSG-2 (Boscher et al., 2012) (Jiang et al., 2014). Furthermore, considering the roles of Gal-3 in binding to several glycoproteins in the ECM via complex and context-dependent mechanisms (Song & Zhang, 2020), it is possible to hypothesise that Gal-3 is an important mediator of cardiomyocyte adhesion and desmosome integrity in the heart. Therefore, along with the canonical Wnt pathway suppressive effects of Gal-3 mutation, it can be speculated that the desmosome instability caused by Gal-3 deficiency activates the Hippo pathway, thus leading to pro-adipogenic signalling as described in section 1.2.2. The overall effects of this phenomena have been extensively demonstrated by Chen et al. In fact, cytoplasmic YAP retention upon Hippo pathway activation not only inhibits the expression of downstream YAP target genes by suppressing YAP/TEAD transcriptional activities, but also leads to β-catenin degradation and subsequent reduction in β-catenin/TCF transcriptional activities. All together, these mechanisms promote adipogenic, fibrogenic and apoptotic pathways while hindering cardiomyocyte growth and survival. Indeed, our results show that the YAP-TAZ target gene *ccn2b* is downregulated in *lgals3a* -/- larvae (Figure 3.7), supporting the hypothesis that Gal-3 is involved in maintaining the structural integrity of the desmosomes and its loss of function induces Hippo activation and the subsequent events leading to AC-related phenotypes. We also observed the *ccn2a* isoform to be slightly downregulated. This difference is attributable to their expressional regulation at different time points during Hippo ON state. It was demonstrated that *ccn2a* mRNA levels were much higher compared to *ccn2b* upon cardiac damage. These researchers concluded that ccn2a is involved in cardiac regeneration by promoting cardiomyocyte proliferation, without making an emphasis on its regulation by YAP-TAZ Hippo effectors.

As aforementioned, AC manifestation is strongly linked to desmosome instability. In this context, our results are in agreement with Cason et al. findings by having demonstrated that truncated Gal-3 leads to a reduction in the expression of both Dsp protein isoforms at the whole body level (Figure 3.4), although this observation alone is not sufficient to hypothesise any disease-related mechanism. Interestingly, our data shows that Gal-3 deficiency not only interferes with this protein's

expression but also resulted in the downregulation of mRNA expression of *dspa* isoform in zebrafish (not shown). This can be attributed to the mRNA stability and pre-mRNA splicing roles of Gal-3 in the nucleus (Newlaczyl & Yu, 2011).

Wnt signalling suppression was coupled with developmental delay of the mutant larvae, where both the metrics typically used to gauge zebrafish growth- body length and eye size- were significantly reduced (Figure 3.10). This finding was not a surprise considering the importance of canonical Wnt signalling in growth and development, and the regulatory roles of Gal-3 on this pathway. Intriguingly, the reduction of the dimensions of *lgals3a* -/- larvae, a factor that may have potentially affected the proportions of the organs, did not involve the cardiac region. Instead, a dilation was observed in mutants compared to the WT condition (Figure 3.8). This dilation is in fact associated with the loss of structural integrity of the cardiomyocytes and weakened intercellular junctions at the IDs, resulting - along with the low levels of Wnt signalling expression - in morphological changes such as pericardial oedema and blood effusion. Therefore, the ultimate outcome is the overall enlargement of the cardiac region. Notably, the observed dilation was maintained from larval stage (by evaluating the overall heart size) to adulthood (based on the ventricle dimension) (Figures 3.12 and 3.13). This indicates a progression of the phenotype and is correlated with late stage severe biventricular AC in humans. In addition, comparing the degree of cardiac dilation at two different developmental stages of the zebrafish, our results illustrate a heart area that is almost doubled in mutant adult hearts, whereas this difference was not as remarkable at the larval stage. Indeed, this is strictly linked to the continuous remodelling of the heart, worsening of the pathophysiological state and progression of the disease with an age-related penetrance. Moreover, by considering the intrinsic variability of the cardiac region alterations at the larval stage and the fraction of mutant larvae that displayed such aberrant phenotypes (35%) (Figure 3.9), the incompletely penetrant presentation of AC was recapitulated. In fact, most *lgals3a* -/- larvae did not possess an overt phenotype. This outcome indicates a variable influence provided by the 4-bp deletion of the *lgals3a* gene in homozygosity, based on the phenotypic condition that mutant zebrafish displayed. Along with the observed cardiac defects, our results suggest a trend of bradycardia in *lgals3a* -/- zebrafish at every stage of development considered (Figure 3.11). This reduction in the heart rate -being the most severe at 5 dpf- indicates a potential structural instability of the heart that is negatively affecting the transmission of the contraction signal, thereby causing electrophysiological abnormalities in the heart. Moreover, survival analysis revealed a shorter life expectancy of *lgals3a* -/- zebrafish with respect to the WT controls (Figure 3.16). This result is consistent with the other findings that demonstrate morphological alterations, signalling pathway dysregulations and cardiac cell death. Thereby, it is unquestionable that the abnormalities occurring at the level of key signalling pathways and the resulting phenotypic conditions due to Gal-3 deficiency in mutant larvae collectively

influence the survival rate. Of note, the emergence of death events in larvae at about 9-10 dpf possibly marks a developmental stage that may be referred to as a general and critical limit for the livelihood of the zebrafish model.

Another important finding was the presence of cell death in the cardiac region of *lgals3a* mutant larvae, a clear marker of AC onset. In this setting, *lgals3a* -/- larvae were shown to exhibit apoptotic/necrotic features, confirmed by the quantification of acridine orange fluorescent staining, which was higher than that of the WT larvae (Figure 3.15). Indeed, a typical cardiac cycle exposes the myocardium to mechanical stress and, when under such load, compromised cardiac desmosomes are unable to maintain adequate cell-cell adhesion, which leads to desmosome collapse and progressive cardiomyocyte death by activation of programmed and unprogrammed cell death pathways, such as apoptosis or necroptosis. In this context, our results clearly demonstrated the suppression of the canonical Wnt pathway (Figure 3.5 and 3.6) and reduction of Dsp protein expression (Figure 4.3) in response to *lgals3a* mutation, as supported by previous findings (Cason et al., 2021). Both phenomena have been implicated in the loss of cardiomyocytes; DSP mutations cause the loss of desmosome integrity and weakened ID intercellular junctions (Yuan et al., 2021) (i.e. Wnt pathway downregulation by JUP release), while Wnt pathway suppression leads to downregulation of myogenesis and upregulation of apoptosis/adipogenesis (Hoorntje et al., 2017). Therefore, it is possible to postulate that truncated Gal-3 triggers cell death mechanisms via dysregulating the canonical Wnt/β-catenin pathway and widening the desmosome gaps depending on DSP and DSG-2.

Furthermore, it has been established that myocardial fibrosis in AC is preceded by inflammation (Meraviglia et al., 2021). In accordance with this, along with necrosis and apoptosis, damage by inflammation is thought to be another factor contributing to the cardiomyocyte loss and AC pathogenesis (Yuan et al., 2021). Indeed, AC post-mortem histological samples reveal the presence of inflammatory cell infiltrates in the areas of fibrosis. In addition, this immune response is mostly as a result of necrosis in the myocardial tissue. Therefore, as a preliminary assessment, L-plastin specific cells were detected through immunofluorescence analysis in to reveal the number of leukocytes present in WT and *lgals3a* -/- larvae (Figure 3.14). Although our results were statistically not significant, there was a trend towards an increase in L-plastin expression in mutant larvae compared to the WT condition. Indeed, inflammation can be favoured by the suppression of the Wnt signalling, Hippo pathway activation, the morphological changes observed at different developmental stages, increased cell death and the supposed desmosome instability. Thereby, the observed dysregulations at different levels can collectively lead to inflammation at 3 dpf. However, Gal-3 is known to be a pro-inflammatory protein upon its prolonged overexpression, by extensively regulating the innate immune response and pro-fibrotic pathways (e.g. alternative macrophage activation)

(Henderson & Sethi, 2009). In fact, ventricular remodelling in human HF is associated with Gal-3 systemic increase. Therefore, it can be speculated that under normal conditions, Gal-3 has a protective role in the heart through regulating the canonical Wnt signalling, and possessing cell-cell/cell-matrix adhesion and anti-apoptotic/anti-necrotic properties; hence, its suppression can result in AC disease onset. However, under pathological conditions (i.e. desmosome mutation), Gal-3 serum concentration increases along with its synthesis and secretion (Cason et al., 2021), promoting disease progression.

5. CONCLUSIONS AND FUTURE PERSPECTIVES

The present study was designed to determine the effect of truncated Gal-3 in AC disease context. Our data suggest a critical role played by Gal-3 in the regulation of the canonical Wnt/β-catenin signalling- the key molecular mechanism associated with AC manifestation. Gal-3 deficiency led to significant morphological defects (i.e. cardiac dilation, oedema and blood effusion) and developmental delay, addressing the implication of Gal-3 in the development of zebrafish and its heart. Moreover, truncated Gal-3 led to the activation of the Hippo pathway and reduced expression of Dsp, both of which are currently considered pathological conditions in AC. Gal-3 mutation also induced cell death in the cardiac region, which is an indication of cardiomyocyte loss. On the other hand, Gal-3 is known to promote inflammation and fibrosis- the two main contributors of disease progression in AC. Since zebrafish Gal-3 mutants seems to display increased inflammation at the cardiac level, it is tempting to speculate that Gal-3 amounts, both at high and low levels, could be critical in regulating the inflammatory process. Further analysis, modulating Gal-3, either overexpressing or downregulating it, could clarify this aspect. Taken together, the principal theoretical implication of this study is that Gal-3 mutations might contribute to AC pathogenesis during the latent phase by altering key signalling pathways, before the overt progressive stage characterised by the fibro-fatty replacement of the ventricular myocardium.

A limitation of this study is that it was not possible to assess the level of Gal-3 protein due to the unavailability of a working antibody for zebrafish. Therefore, C-terminal truncation is still awaiting experimental confirmation. Furthermore, the small sample size did not allow to draw accurate conclusions on whether inflammation is present in the mutant larvae or not. Other limiting factors were the lack of information on the *lgals3b* gene and the limited number of eggs obtained from the *lgals3b* -/- zebrafish, compromising the possibility of conducting more in-depth analyses and the generation of double heterozygotes. In spite of these limitations, the study certainly adds to our understanding of Gal-3 and its possible involvement in AC manifestation.

Further studies need to be carried out to validate the effect of Gal-3 mutations on desmosome destabilisation in the heart. In this sense, JUP release and its accumulation in the cytoplasm should be carefully assessed wherein continued efforts are needed to make antibodies more accessible for zebrafish studies. There is also a need for TEM (transmission electron microscopy) analysis to explore the structural alterations at the desmosome level. Moreover, further work could assess the long-term effects of Gal-3 mutations by histological analysis, to shed more light

on the presence of fibro-adipose tissue in the ventricular myocardium of the zebrafish, if any, although an additional uncontrolled factor would be the regeneration capacity of zebrafish. To examine a possible inflammation, necrotic cell death specific experiments should be conducted. Investigation and experimentation into Gal-3-Dsp double mutants is also strongly recommended to determine the implication of Gal-3 in the AC zebrafish model. Furthermore, it would also be interesting to perform sophisticated electrophysiological experiments to provide more insights into the extent of arrhythmic episodes observed.

A natural progression of this work is to evaluate if treatment with SB216763, a Wnt agonist, is able to ameliorate the negative effects of Gal-3 mutations in zebrafish through the upregulation of the Wnt/β-catenin signalling. In this context, assessing the effect of intensive training in treated vs control zebrafish would be of great help in determining the change in the anatomy of tissues upon exercise and the recovery provided by the drug, if any. This information can be used to develop targeted interventions aimed at upregulating the Wnt signal, since Gal-3 mutations also lead to a strong suppression of this pathway.

Understanding the implication of Gal-3 in the pathogenesis of AC, will facilitate the development of Gal-3 inhibitors, since both reduced (i.e. suppression of its function) and increased Gal-3 expression in early and advanced stages of disease, respectively, appear to be contributing factors of AC onset and progression.

REFERENCES

1- All about Zebra Fish: Characteristics, habitat, employ in labs and more... (2019, April 11). Discovering All Marine Species. https://ourmarinespecies.com/wp-content/cache/page_enhanced/ourmarinespecies.com/c-fishes/all-about-zebra-fish/_index.html_gzip

2- Argüeso, P., Mauris, J., & Uchino, Y. (2015). Galectin-3 as a regulator of the epithelial junction: Implications to wound repair and cancer. Tissue Barriers, 3(3), e1026505. https://doi.org/10.1080/21688370.2015.1026505

3- Asimaki, A., Kapoor, S., Plovie, E., Karin Arndt, A., Adams, E., Liu, Z., James, C. A., Judge, D. P., Calkins, H., Churko, J., Wu, J. C., MacRae, C. A., Kléber, A. G., & Saffitz, J. E. (2014). Identification of a New Modulator of the Intercalated Disc in a Zebrafish Model of Arrhythmogenic Cardiomyopathy. Science Translational Medicine, 6(240). https://doi.org/10.1126/scitranslmed.3008008

4- Austin, K. M., Trembley, M. A., Chandler, S. F., Sanders, S. P., Saffitz, J. E., Abrams, D. J., & Pu, W. T. (2019). Molecular mechanisms of arrhythmogenic cardiomyopathy. Nature Reviews Cardiology, 16(9), 519–537. https://doi.org/10.1038/s41569-019-0200-7

5- Boscher, C., Zheng, Y. Z., Lakshminarayan, R., Johannes, L., Dennis, J. W., Foster, L. J., & Nabi, I. R. (2012). Galectin-3 Protein Regulates Mobility of N-cadherin and GM1 Ganglioside at Cell-Cell Junctions of Mammary Carcinoma Cells. Journal of Biological Chemistry, 287(39), 32940–32952. https://doi.org/10.1074/jbc.m112.353334

6- Calore, M., Lorenzon, A., De Bortoli, M., Poloni, G., & Rampazzo, A. (2014). Arrhythmogenic cardiomyopathy: a disease of intercalated discs. Cell and Tissue Research, 360(3), 491–500. https://doi.org/10.1007/s00441-014-2015-5

7- Cason, M., Celeghin, R., Marinas, M. B., Beffagna, G., Della Barbera, M., Rizzo, S., Remme, C. A., Bezzina, C. R., Tiso, N., Bauce, B., Thiene, G., Basso, C., & Pilichou, K. (2021). Novel pathogenic role for galectin-3 in early disease stages of arrhythmogenic cardiomyopathy. Heart Rhythm, 18(8), 1394–1403. https://doi.org/10.1016/j.hrthm.2021.04.006

8- Chelko, S. P., Asimaki, A., Andersen, P., Bedja, D., Amat-Alarcon, N., DeMazumder, D., Jasti, R., MacRae, C. A., Leber, R., Kleber, A. G., Saffitz, J. E., & Judge, D. P. (2016). Central role for GSK3β in the pathogenesis of

arrhythmogenic cardiomyopathy. JCI Insight, 1(5). https://doi.org/10.1172/jci.insight.85923

9- Chen, K., Fan, Y., Gu, J., Han, Z., Wang, Y., Gao, L., Zeng, H., Mao, C., & Wang, C. (2021). Effect of lgals3a on embryo development of zebrafish. Transgenic Research, 30(6), 739–750. https://doi.org/10.1007/s11248-021-00276-5

10- Chen, S. N., Gurha, P., Lombardi, R., Ruggiero, A., Willerson, J. T., & Marian, A. J. (2014). The Hippo Pathway Is Activated and Is a Causal Mechanism for Adipogenesis in Arrhythmogenic Cardiomyopathy. Circulation Research, 114(3), 454–468. https://doi.org/10.1161/circresaha.114.302810

11- Colin Hughes, R. (2001). Galectins as modulators of cell adhesion. Biochimie, 83(7), 667–676. https://doi.org/10.1016/s0300-9084(01)01289-5

12- Corrado, D., Basso, C., & Judge, D. P. (2017). Arrhythmogenic Cardiomyopathy. Circulation Research, 121(7), 784–802. https://doi.org/10.1161/circresaha.117.309345

13- Dumic, J., Dabelic, S., & Flögel, M. (2006). Galectin-3: An open-ended story. Biochimica et Biophysica Acta (BBA) - General Subjects, 1760(4), 616–635. https://doi.org/10.1016/j.bbagen.2005.12.020

14- Facchinello, N., Tarifeño-Saldivia, E., Grisan, E., Schiavone, M., Peron, M., Mongera, A., Ek, O., Schmitner, N., Meyer, D., Peers, B., Tiso, N., & Argenton, F. (2017). Tcf7l2 plays pleiotropic roles in the control of glucose homeostasis, pancreas morphology, vascularization and regeneration. Scientific Reports, 7(1). https://doi.org/10.1038/s41598-017-09867-x

15- Garrod, D., & Chidgey, M. (2008). Desmosome structure, composition and function. Biochimica et Biophysica Acta (BBA) - Biomembranes, 1778(3), 572–587. https://doi.org/10.1016/j.bbamem.2007.07.014

16- Henderson, N. C., & Sethi, T. (2009). The regulation of inflammation by galectin-3. Immunological Reviews, 230(1), 160–171. https://doi.org/10.1111/j.1600-065x.2009.00794.x

17- Hoorntje, E. T., te Rijdt, W. P., James, C. A., Pilichou, K., Basso, C., Judge, D. P., Bezzina, C. R., & van Tintelen, J. P. (2017). Arrhythmogenic cardiomyopathy: pathology, genetics, and concepts in pathogenesis. Cardiovascular Research, 113(12), 1521–1531. https://doi.org/10.1093/cvr/cvx150

18- Hsu, D. K., & Liu, F.-T. (2002). Regulation of cellular homeostasis by galectins. Glycoconjugate Journal, 19(7-9), 507–515. https://doi.org/10.1023/b:glyc.0000014080.95829.52

19- Jiang, K., Rankin, C. R., Nava, P., Sumagin, R., Kamekura, R., Stowell, S. R., Feng, M., Parkos, C. A., & Nusrat, A. (2014). Galectin-3 Regulates Desmoglein-2 and Intestinal Epithelial Intercellular Adhesion. Journal of Biological Chemistry, 289(15), 10510–10517. https://doi.org/10.1074/jbc.m113.538538

20- Johannes, L., Jacob, R., & Leffler, H. (2018). Galectins at a glance. Journal of Cell Science, 131(9), jcs208884. https://doi.org/10.1242/jcs.208884

21- Lorenzon, A., Calore, M., Poloni, G., De Windt, L. J., Braghetta, P., & Rampazzo, A. (2017). Wnt/β-catenin pathway in arrhythmogenic cardiomyopathy. Oncotarget, 8(36), 60640–60655. https://doi.org/10.18632/oncotarget.17457

22- Meraviglia, V., Alcalde, M., Campuzano, O., & Bellin, M. (2021). Inflammation in the Pathogenesis of Arrhythmogenic Cardiomyopathy: Secondary Event or Active Driver? Frontiers in Cardiovascular Medicine, 8. https://doi.org/10.3389/fcvm.2021.784715

23- Migliore, F., Mattesi, G., Zorzi, A., Bauce, B., Rigato, I., Corrado, D., & Cipriani, A. (2021). Arrhythmogenic Cardiomyopathy—Current Treatment and Future Options. Journal of Clinical Medicine, 10(13), 2750. https://doi.org/10.3390/jcm10132750

24- Moro, E., Vettori, A., Porazzi, P., Schiavone, M., Rampazzo, E., Casari, A., Ek, O., Facchinello, N., Astone, M., Zancan, I., Milanetto, M., Tiso, N., & Argenton, F. (2013). Generation and application of signaling pathway reporter lines in zebrafish. Molecular Genetics and Genomics, 288(5-6), 231–242. https://doi.org/10.1007/s00438-013-0750-z

25- Newlaczyl, A. U., & Yu, L.-G. (2011). Galectin-3 – A jack-of-all-trades in cancer. Cancer Letters, 313(2), 123–128. https://doi.org/10.1016/j.canlet.2011.09.003

26- Pilichou, K., Thiene, G., Bauce, B., Rigato, I., Lazzarini, E., Migliore, F., Perazzolo Marra, M., Rizzo, S., Zorzi, A., Daliento, L., Corrado, D., & Basso, C. (2016). Arrhythmogenic cardiomyopathy. Orphanet Journal of Rare Diseases, 11, 33. https://doi.org/10.1186/s13023-016-0407-1

27- Rampazzo, A., Calore, M., van Hengel, J., & van Roy, F. (2014). Intercalated Discs and Arrhythmogenic Cardiomyopathy. Circulation: Cardiovascular Genetics, 7(6), 930–940. https://doi.org/10.1161/circgenetics.114.000645

28- Sciacchitano, S., Lavra, L., Morgante, A., Ulivieri, A., Magi, F., De Francesco, G., Bellotti, C., Salehi, L., & Ricci, A. (2018). Galectin-3: One Molecule for an Alphabet of Diseases, from A to Z. International Journal of Molecular Sciences, 19(2), 379. https://doi.org/10.3390/ijms19020379

29- Shimura, T., Takenaka, Y., Fukumori, T., Tsutsumi, S., Okada, K., Hogan, V., Kikuchi, A., Kuwano, H., & Raz, A. (2005). Implication of Galectin-3 in Wnt Signaling. Cancer Research, 65(9), 3535–3537. https://doi.org/10.1158/0008-5472.can-05-0104

30- Shimura, T., Takenaka, Y., Tsutsumi, S., Hogan, V., Kikuchi, A., & Raz, A. (2004). Galectin-3, a Novel Binding Partner of β-Catenin. Cancer Research, 64(18), 6363–6367. https://doi.org/10.1158/0008-5472.can-04-1816

31- Song, R., & Zhang, L. (2020). Cardiac ECM: Its Epigenetic Regulation and Role in Heart Development and Repair. International Journal of Molecular Sciences, 21(22), 8610. https://doi.org/10.3390/ijms21228610

32- Song, S., Mazurek, N., Liu, C., Sun, Y., Ding, Q. Q., Liu, K., Hung, M.-C., & Bresalier, R. S. (2009). Galectin-3 Mediates Nuclear β-Catenin Accumulation and Wnt Signaling in Human Colon Cancer Cells by Regulation of Glycogen Synthase Kinase-3β Activity. Cancer Research, 69(4), 1343–1349. https://doi.org/10.1158/0008-5472.can-08-4153

33- Sygitowicz, G., Maciejak-Jastrzębska, A., & Sitkiewicz, D. (2021). The Diagnostic and Therapeutic Potential of Galectin-3 in Cardiovascular Diseases. Biomolecules, 12(1), 46. https://doi.org/10.3390/biom12010046

34- Yang, R.-Y., Rabinovich, G. A., & Liu, F.-T. (2008). Galectins: structure, function and therapeutic potential. Expert Reviews in Molecular Medicine, 10. https://doi.org/10.1017/s1462399408000719

35- Yuan, Z.-Y., Cheng, L.-T., Wang, Z.-F., & Wu, Y.-Q. (2021). Desmoplakin and clinical manifestations of desmoplakin cardiomyopathy. Chinese Medical Journal, 134(15), 1771–1779. https://doi.org/10.1097/CM9.0000000000001581